50. Koike, M. *et al.* Cathepsin D deficiency induces lysosomal storage with ceroid lipofuscin in mouse CNS neurons. *J. Neurosci.* **20,** 6898–6906 (2000).
51. Mori, Y. *et al.* Human herpesvirus-6 induces MVB formation, and virus egress occurs by an exosomal release pathway. *Traffic* **9,** 1728–1742 (2008).
52. Wang, G. H. *et al.* Caspase activation during apoptotic cell death induced by expanded polyglutamine in N2a cells. *Neuroreport* **10,** 2435–2438 (1999).
53. Yamanaka, T. *et al.* Lgl mediates apical domain disassembly by suppressing the PAR-3-aPKC-PAR-6 complex to orient apical membrane polarity. *J. Cell Sci.* **119,** 2107–2118 (2006).

Acknowledgements

We thank Dr Shigeyoshi Itohara (RIKEN BSI) for RNZ mice and Dr Jun-ichi Miyazaki (Osaka University) for CAG-cre mice, Dr Tomonori Hirose (Yokohama City University) for mice technical information, Dr Koji Yamanaka for critical suggestion for manuscript preparation, the staff at the RRC (RIKEN BSI) for technical support, the FANTOM consortium for FANTOM clones, and lab members of RIKEN BSI for technical help. This work was supported by a Grant-in-Aid from Ministry of Education, Culture, Sports, Science and Technology (MEXT) of Japan for T.Y. (24111553 for Scientific Research on Innovative Areas 'Brain Environment', 23700430, Comprehensive Brain Science Network) and N.N. (22110004 for Scientific Research on Innovated Areas 'Foundation of Synapse and Neurocircuit Pathology', 22240037, 24659436, 25253066), by CREST from JST for N.N. and by Grant-in-Aid for the Research on Measures for Ataxic Diseases from the Ministry of Health, Welfare and Labor for N.N.

Author contributions

T.Y. and A.T. mainly performed the experiments; M.K. conducted some of the mouse work; G.M. generated Derlin1-RFP cells; M.K and Y.U. conducted EM; S.N.M. generated NF-YA flox mice; T.Y., N.H., T.S. and N.N. analysed the data, and T.Y. and N.N. designed the experiments and wrote the manuscript.

Additional information

Supplementary Information accompanies this paper at http://www.nature.com/naturecommunications

Competing financial interests: The authors declare no competing financial interests.

Reprints and permission information is available online at http://npg.nature.com/reprintsandpermissions/

How to cite this article: Yamanaka, T. *et al.* NF-Y inactivation causes atypical neurodegeneration characterized by ubiquitin and p62 accumulation and endoplasmic reticulum disorganization. *Nat. Commun.* 5:3354 doi: 10.1038/ncomms4354 (2014).

© 2014 Macmillan Publishers Limited. All rights reserved.

OPEN ACCESS Freely available online

PLOS ONE

p150^{glued}-Associated Disorders Are Caused by Activation of Intrinsic Apoptotic Pathway

Kei-Ichi Ishikawa[1], Shinji Saiki[1], Norihiko Furuya[1,2], Daisuke Yamada[1], Yoko Imamichi[1], Yuanzhe Li[1], Sumihiro Kawajiri[1], Hironori Sasaki[1], Masato Koike[3], Yoshio Tsuboi[4], Nobutaka Hattori[1,2]*

1 Department of Neurology, Juntendo University School of Medicine, Tokyo, Japan, **2** Department of Research and Therapeutics for Movement Disorders, Juntendo University School of Medicine, Tokyo, Japan, **3** Department of Cell Biology and Neuroscience, Juntendo University School of Medicine, Tokyo, Japan, **4** Department of Neurology, Fukuoka University School of Medicine, Fukuoka, Japan

Abstract

Mutations in p150^{glued} cause hereditary motor neuropathy with vocal cord paralysis (HMN7B) and Perry syndrome (PS). Here we show that both overexpression of p150^{glued} mutants and knockdown of endogenous p150^{glued} induce apoptosis. Overexpression of a p150^{glued} plasmid containing either a HMN7B or PS mutation resulted in cytoplasmic p150^{glued}-positive aggregates and was associated with cell death. Cells containing mutant p150^{glued} aggregates underwent apoptosis that was characterized by an increase in cleaved caspase-3- or Annexin V-positive cells and was attenuated by both zVAD-fmk (a pan-caspase inhibitor) application and caspase-3 siRNA knockdown. In addition, overexpression of mutant p150^{glued} decreased mitochondrial membrane potentials and increased levels of translocase of the mitochondrial outer membrane (Tom20) protein, indicating accumulation of damaged mitochondria. Importantly, siRNA knockdown of endogenous p150^{glued} independently induced apoptosis via caspase-8 activation and was not associated with mitochondrial morphological changes. Simultaneous knockdown of endogenous p150^{glued} and overexpression of mutant p150^{glued} had additive apoptosis induction effects. These findings suggest that both p150^{glued} gain-of-toxic-function and loss-of-physiological-function can cause apoptosis and may underlie the pathogenesis of p150^{glued}-associated disorders.

Citation: Ishikawa K-I, Saiki S, Furuya N, Yamada D, Imamichi Y, et al. (2014) p150^{glued}-Associated Disorders Are Caused by Activation of Intrinsic Apoptotic Pathway. PLoS ONE 9(4): e94645. doi:10.1371/journal.pone.0094645

Editor: Hiroyoshi Ariga, Hokkaido University, Japan

Received December 2, 2013; **Accepted** March 18, 2014; **Published** April 10, 2014

Copyright: © 2014 Ishikawa et al. This is an open-access article distributed under the terms of the Creative Commons Attribution License, which permits unrestricted use, distribution, and reproduction in any medium, provided the original author and source are credited.

Funding: The authors are grateful for these 9 grants: the Grant from the Japanese Ministry of Health, Labour and Welfare (http://www.mhlw.go.jp/stf/seisakunitsuite/bunya/hokabunya/kenkyujigyou/index.html) (N.H.), the Grant-in-Aid for Young Scientists (A) (S.S.), the Grant-in-Aid for Scientific Research (C) (N.F.), the Grant-in-Aid for Challenging Exploratory Research (S.S.) from Japan Society for the Promotion of Science (http://www.jsps.go.jp/index.html), Grant-in-Aid for Scientific Research on Priority Areas (S.S.) from Japanese Ministry of Education, Culture, Sports, Science and Technology (http://www.mext.go.jp/a_menu/shinkou/hojyo/main5_a5.htm), and grants from the Life Science Foundation (http://www.lifesci-found.com/), the Takeda Scientific Foundation (http://www.takeda-sci.or.jp/), the Cell Science Research Foundation (http://www.shionogi.co.jp/zaidan/), and the Nakajima Foundation (http://www.nakajimafound.or.jp/index.html) (S.S.). The funders had no role in study design, data collection and analysis, decision to publish, or preparation of the manuscript.

Competing Interests: The authors have declared that no competing interests exist.

* E-mail: nhattori@juntendo.ac.jp

Introduction

The dynactin subunit p150^{glued} is encoded by the *DCTN1* gene. Mutations in this gene have been detected in patients with slowly progressive autosomal dominant distal hereditary motor neuropathy with vocal cord paralysis (HMN7B) and autosomal dominant Perry syndrome (PS), the latter of which is characterized by rapidly progressive, devastating neurodegeneration of dopaminergic neurons in the substantia nigra [1,2].

Dynactin has various molecular functions including minus-end vesicular transport, protein degradation, and cell division. p150^{glued} is the largest polypeptide of the dynactin complex, and it binds directly to microtubules and to cytoplasmic dynein. Disruption of the p150^{glued} CAP-Gly domain in neurons causes insufficient retrograde axonal transport [3,4]. Transgenic mice expressing p150^{glued} with a G59S mutation develop progressive degeneration of motor neurons similar to that seen in amyotrophic lateral sclerosis [5–7]. The mutated p150^{glued} polypeptide that causes PS is unable to bind to microtubules and forms intracytoplasmic aggregates. These aggregates include abnormally accumulated mitochondria [11]. Despite these findings, it is unclear whether decreased levels of endogenous p150^{glued} or increased levels of the mutant form dominantly contribute to the neurodegeneration seen in PS.

Here we report that knockdown of endogenous p150^{glued} and overexpression of p150^{glued} with pathogenic HMN7B or PS mutations independently induced apoptosis. However, only overexpression of mutant forms of p150^{glued} induced intracytoplasmic p150^{glued}-aggregates and accumulation of damaged mitochondria, resulting in intrinsic apoptosis induction. Importantly, mutant p150^{glued} overexpression with endogenous p150^{glued} knockdown showed additive effects on apoptosis induction, suggesting that both a gain- and loss-of-function contribute to the disease pathogenesis.

Results

Cells overexpressing various p150^{glued} mutants produce cytoplasmic aggregates

To investigate the effects of overexpression of mutant p150^{glued}, we first generated plasmid DNAs encoding GFP- or 3xFLAG-tagged wild-type (WT) and mutant p150^{glued} with each pathogenic mutation: G59S, which causes HMN7B, and G71A, G71E,

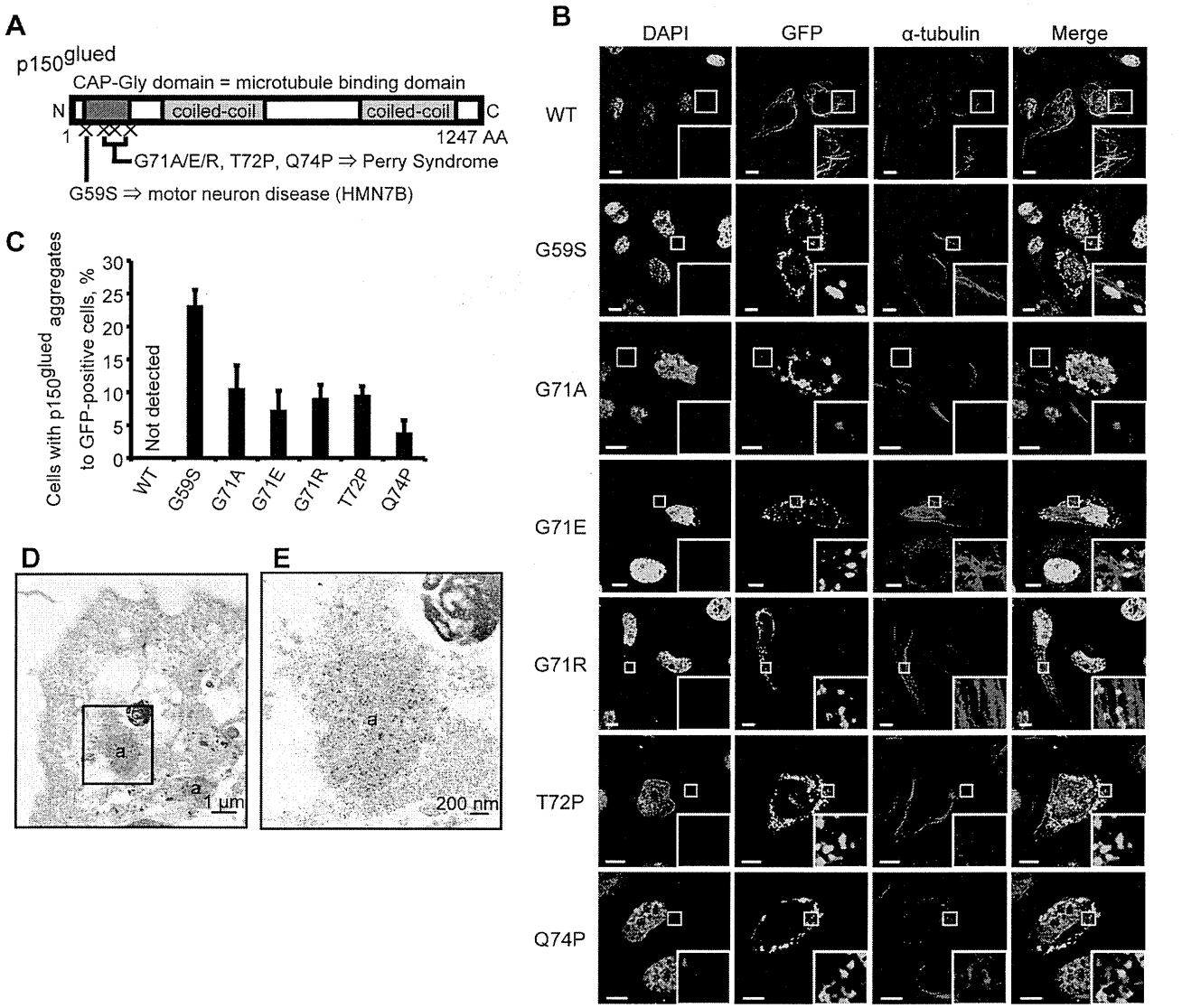

Figure 1. Disease-associated p150^{glued} mutant proteins form aggregates. (A) Schematic of the p150^{glued} subunit of dynactin. (B) HeLa cells transfected with GFP-tagged wild-type or mutant p150^{glued} were fixed and stained with an antibody against α-tubulin (red) after 24 h and analyzed using confocal microscopy. Insets show higher magnification of the boxed areas. Bars, 10 μm. (C) The percentages of GFP-positive cells that contained aggregates are shown. The error bar indicates each standard deviation. Statistics are from three independent experiments. (D, E) Electron micrographic examination of HeLa cells transfected with GFP-tagged G59S p150^{glued} and immunolabeled with an antibody against GFP. (E) High magnification of the boxed area shown in (D). Intracytoplasmic aggregates (a) are labeled.
doi:10.1371/journal.pone.0094645.g001

G71R, T72P, or Q74P, which cause PS. All of these mutations are within the p150^{glued} CAP-Gly microtubule binding domain (Figure 1A).

To determine if a mutation in p150^{glued} affected its intracellular localization, we transfected GFP-tagged WT or mutant p150^{glued} into HeLa cells followed by immunocytochemical analysis. HeLa cells overexpressing GFP-WT p150^{glued} showed complete colocalization with tubulin (Figure 1B). By contrast, those with a pathogenic mutation were diffusely distributed in the cytoplasm and showed no apparent colocalization with tubulin (Figure S1A). Additionally, cytoplasmic, but not nuclear, aggregates were observed in cells with high expression levels of the mutant p150^{glued} plasmids as early as 24 h after transfection, most frequently in the perinuclear region of the cells with G59S p150^{glued} (Figure 1B, C). These findings are consistent with previous reports [8,11]. Analogous results were detected with the overexpression of 3xFLAG-tagged WT and mutant p150^{glued} in SH-SY5Y (Figure S1B) and HeLa cells (Figure S1C, D). Previous studies examining the overexpression of mutant G59S p150^{glued} showed decreased affinity of the mutant form of p150^{glued} for microtubules, indicating that mutant p150^{glued} dissociated from microtubules and formed aggregates [11].

To confirm the formation of cytoplasmic aggregates, we performed conventional electron microscopy (EM) analysis. High-density aggregates around the nuclei were detected in cells overexpressing G59S or G71R p150^{glued} (Figure S1E). Next, using immuno-EM analysis with anti-GFP antibodies to recognize GFP-tagged mutant p150^{glued}, we detected p150^{glued} localized in high

density aggregates, particularly in the perinuclear region of the cells overexpressing G59S (Figure 1D, E) or G71R (data not shown) p150^{glued}. Unfortunately, because of the fixation technique for immuno-EM, we could not use the same specimens to assess morphological changes in organelles, including mitochondria, in the cells that showed the aggregates.

We next sought to determine the characteristics of the aggregates by immunocytochemistry. The mutant p150^{glued} aggregates were partially positive for endogenous ubiquitin but not for FLAG-tagged TAR DNA-binding protein 43 (TDP-43) (Figure S1F, G). This is consistent with previous reports showing that dynactin subunits p50 and p62 were present in less than 5% of TDP-43-expressing neurons in the globus pallidus of the autopsied brain of a PS patient [8].

Apoptotic changes occurred in cells with cytoplasmic aggregates

To elucidate the pathogenesis of the p150^{glued}-associated diseases, we focused on the association of cytoplasmic aggregates induced by mutant p150^{glued} overexpression with cell death. We tested the death rate of cells expressing the GFP-tagged p150^{glued}, assessed by nuclear morphological changes described in a previous report [12]. The rate of cell death was significantly increased by overexpression of G59S or G71R p150^{glued} both 24 and 48 h after transfection when compared with control cells (Figure 2A).

To examine the characteristics of the cell death induced by G59S or G71R p150^{glued}, we performed the same analysis 24 h after transfection with controls cells and cells treated with the pan-caspase inhibitor carbobenzoxy-valyl-alanyl-aspartyl-[O-methyl]-fluoromethylketone (z-VAD-fmk). The rate of cell death induced by overexpression of G59S or G71R p150^{glued} was significantly suppressed by z-VAD (Figure 2B) [13]. In a population of cells selected based on GFP (p150^{glued}) intensity, the numbers of early apoptotic cells (annexin V-positive, propidium iodide (PI)-negative) and late apoptotic or necrotic cells (annexin V-positive, PI-positive) were both increased by overexpression of G59S or G71R p150^{glued} (Figure 2C, D). Likewise, z-VAD treatment significantly decreased cell death in both G59S and G71R p150^{glued}-overexpressing cells.

To examine the activation of the intrinsic apoptotic pathway, we determined whether or not cells with aggregates were positive for cleaved caspase-3 using fluorescent-activated cell sorting (FACS) and immunocytochemistry analyses. The number of cells positive for both cleaved caspase-3 and GFP (p150^{glued}) in cells overexpressing G59S or G71R p150^{glued} was markedly increased compared with control cells (Figure 2E, F). We found that siRNA knockdown against caspase-3 blocked the increase of cell death caused by the overexpression of the mutant p150^{glued} (Figure 2G, H). Next, we wanted to rule out the possibility that extrinsically induced apoptosis via caspase-8 cleavage was causing some or all of the cell death seen in these experiments. Therefore, to exclude this possibility, we examined whether siRNA knockdown of caspase-8 inhibited the apoptosis induced by overexpression of mutant p150^{glued}. Knockdown of caspase-8 did not inhibit apoptosis induced by overexpression of G59S p150^{glued} (Figure S2), suggesting that extrinsically induced apoptosis is not the cause of the cell death seen in these cells.

Aggregate formation caused by the G59S mutant led to cell death. Both aggregate formation and cell death are inhibited by overexpression of Hsp70, a molecular chaperone. These findings suggest that mutant p150^{glued} aggregates play an important role in the mechanism of cell death in HMN7B [11]. We conclude that mutant p150^{glued} aggregates cause apoptosis via activation of the intrinsic apoptotic pathway.

Cells with cytoplasmic aggregates have more mitochondria with reduced mitochondrial membrane potentials

Levy et al. showed that mutant p150^{glued} aggregates are usually associated with mitochondria [11]. Therefore, we hypothesized that an accumulation of damaged mitochondria may cause apoptosis. Live-cell imaging analysis in cells overexpressing WT or mutant p150^{glued} detected elongated tubular mitochondria in control cells, while cells overexpressing mutant p150^{glued} mainly showed fragmented mitochondria in the vicinity of the nuclei (Figure 3A). Overexpression of G59S or G71R p150^{glued} also increased the expression levels of Tom20, a mitochondrial outer membrane protein that is commonly used for assessing mitochondria numbers (Figure 4B, C) [14–16].

To determine the health status of the accumulated mitochondria, we next analyzed cells stained with MitoTracker-Red CMXRos by FACS analysis. Only intact mitochondria with preserved respiration activities and membrane potentials absorb this dye. For an accurate assessment, we only analyzed cells that expressed a high GFP intensity, determined using a flow cytometer. Intriguingly, we detected a marked increase in the number of cells with decreased uptake of MitoTracker-Red CMXRos in cells overexpressing G59S or G71R p150^{glued} compared with the control cells (Figure 3D, E). Also, overexpression of WT p150^{glued} decreased mitochondrial membrane potentials, which might be associated with insufficient mitochondria dynamics [11]. Based on the collected results, we conclude that mutated p150^{glued} causes the accumulation of damaged mitochondria, which is followed by activation of the intrinsic apoptotic pathway.

p150^{glued} knockdown does not affect mitochondrial membrane potentials and activates apoptotic pathway via caspase-8 cleavage

Next, we tested whether or not WT p150^{glued} siRNA knockdown affects mitochondrial functions in a manner similar to mutant p150^{glued} overexpression. As shown in Figure 4A–D, total levels of Tom20 and mitochondria complex I were not changed and the levels of damaged mitochondria without MitoTracker-Red CMX-Ros intake were not significantly increased by p150^{glued} knockdown (Figure 4E, F). Next, we examined caspase-8 activation because of its association with the extrinsic apoptotic pathway. As shown in Figure 5A–H, the levels of total caspase-8 and caspase-3 were decreased with p150^{glued} knockdown, whereas the levels of their cleaved forms of caspase-8 and PARP were increased. This suggests that p150^{glued} knockdown activated caspase-8, leading to caspase-3 activation. Accordingly, treatment with a caspase-8 inhibitor suppressed caspase-3 activation (Figure 5I, J), and caspase-8 siRNA knockdown also decreased apoptotic cell death (Figure 5K, L). Taken together, these data show that the loss-of-function of endogenous p150^{glued} significantly activates caspase-8, inducing apoptosis.

Cells with mutant p150^{glued} overexpression and wild-type endogenous p150^{glued} knockdown showed more apoptosis

Finally, to address the pathogenesis of the p150^{glued}-associated disorders more precisely, we performed mutant p150^{glued} overexpression experiments with or without siRNA knockdown against endogenous p150^{glued}. As shown in Figure 6, siRNA knockdown of endogenous p150^{glued} along with overexpression of either the G59S or G71R mutant form caused many more cells to display early apoptotic changes (GFP-positive and Annexin V-positive)

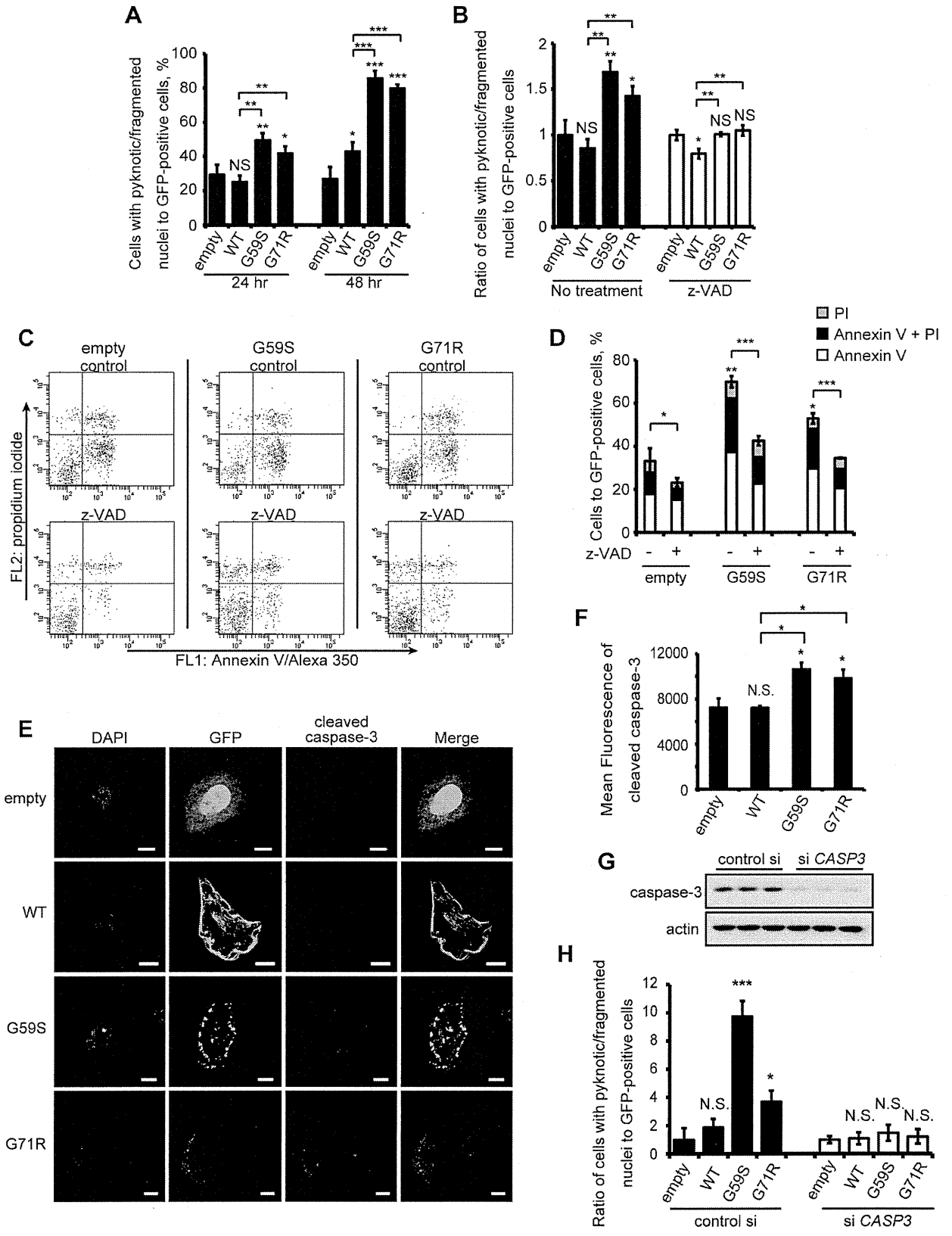

Figure 2. Mutant p150^{glued} proteins activate intrinsic apoptotic pathways. (A) HeLa cells transfected with GFP-empty, GFP-tagged wild-type or mutant (G59S or G71R) p150^{glued} were fixed and stained with DAPI after 24 and 48 h. GFP-positive cells were counted from three independent experiments. The percentage of GFP-positive cells with nuclear abnormalities is shown. (B) Ratio of transfected HeLa cells with nuclear abnormalities

after treatment with or without z-VAD (100 μM) for 24 hours. Values are relative to the GFP-empty value, which is set at 1. (C, D) Transfected SH-SY5Y cells after treatment with or without z-VAD (100 μM) for 48 h were stained with Annexin V and PI, and GFP-positive cells were analyzed by flow cytometry. (E) HeLa cells transfected with GFP-tagged wild-type or mutant p150^{glued} were fixed and stained with an antibody against cleaved caspase-3. Bars, 10 μm. (F) Twenty-four hours after transfection, SH-SY5Y cells were fixed and stained with a cleaved caspase-3 antibody. GFP-positive cells were analyzed by flow cytometry and the mean fluorescent intensity was calculated. (G) HeLa cells were transfected with control scrambled siRNA or caspase-3 siRNA for 72 h and immunoblotting analysis was performed to monitor the knockdown efficiency of the caspase-3 siRNA. (H) Twenty-four hours after transfection with control siRNA or caspase-3 siRNA, HeLa cells were transfected with GFP-empty, GFP-tagged wild-type or mutant p150^{glued}. Forty-eight hours after transfection, cells were fixed and stained with DAPI, and ratios of GFP-positive cells with nuclear abnormalities were analyzed. Values are relative to the GFP-empty value, which is set at 1. The error bar indicates each standard deviation. Statistics are from three independent experiments: N.S., not significant; *, $p<0.05$; **, $p<0.01$; ***, $p<0.001$.
doi:10.1371/journal.pone.0094645.g002

compared with the cells overexpressing a p150^{glued} mutant and a control siRNA. Therefore, we concluded that both excess levels of mutant p150^{glued} and decreased levels of endogenous p150^{glued} contribute to the pathogenesis of p150^{glued}-associated disorders via the activation of apoptosis.

Discussion

In this study, we sought to determine the pathogenesis of p150^{glued}-associated diseases caused by p150^{glued} mutations. Overexpression of mutant p150^{glued} in HeLa and SH-SY5Y cells induced p150^{glued}-positive aggregate formation, accumulation of damaged mitochondria, and activation of the intrinsic apoptotic pathway. Endogenous p150^{glued} knockdown in the same cell lines also activated a caspase-8-dependent apoptotic pathway without apparent mitochondrial abnormalities. Importantly, cell death induced by p150^{glued} knockdown was markedly enhanced by simultaneous overexpression of mutant p150^{glued}, suggesting the disease pathogenesis may be associated with both p150^{glued} gain-of-toxic-function and loss-of-function.

All of the HMN7B and PS associated mutations are located within the CAP-Gly microtubule domain [8], and various reports have suggested that mutant p150^{glued} proteins have the tendency to lose their affinity to microtubules [4,8–10]. Our studies support these reports as we observed decreased colocalization of mutant p150^{glued} with microtubules as well as increased intracytoplasmic aggregates in our immunocytochemistry experiments. However, the *in vivo* binding activity changes of mutant p150^{glued} remain unclear. Therefore, further studies should be performed to determine precisely how mutant p150^{glued} proteins are detoured from their original distribution pattern and how they form aggregates.

The dynein complex plays various critical roles in mitochondrial function (such as retrograde transport and fission/fusion) [17–21]. In this study, we could detect mitochondrial abnormalities (loss of membrane potential and morphological abnormalities) only in cells that expressed mutant forms of p150^{glued}. A report by Varadi et al. found that disruption of dynein function by either p50 overexpression or microinjection of anti-dynein intermediate chain antibodies led to mitochondrial morphology and distribution changes [22]. Our data, however, showed that p150^{glued} siRNA knockdown did not induce mitochondrial abnormalities. Only mutant p150^{glued} overexpression led to these abnormalities, implying that each dynein subunit might have a specific association with mitochondrial function.

Abnormal protein accumulation has been implicated in the pathogenesis of various neurodegenerative diseases [23]. In this study, we revealed that mutant p150^{glued} (G59S, G71R) overexpression induced aggregate formation and caspase activation associated with mitochondrial abnormalities. This supports the findings by Levy et al. who reported that aggregate formation by the G59S mutant leads to cell death, and that both aggregate formation and the induced cell death were inhibited by overexpression of Hsp70, a molecular chaperone [11]. Likewise, other studies have shown that overexpression of a p150^{glued} plasmid with a truncated C-terminal as well as knockdown of endogenous p150^{glued} in rat hippocampal neurons induces caspase-3-positive cell death, which is consistent with our p150^{glued} knockdown results [24,25].

According to studies with *in vivo* models, neither expression of a mutant nor the ΔCAP-Gly domain of p150^{glued} affects axonal transport, but WT p150^{glued} is needed for initiation of retrograde transport at synaptic termini in Drosophila motor neurons and mouse dorsal root ganglion neurons [3,4]. Knock-in and transgenic mice that are heterozygous for the G59S p150^{glued} mutation exhibit late-onset slowly progressive muscle weakness, motor neuron death, and vesicle accumulation [5–7]. This is in contrast to heterozygous p150^{glued} knockout mice, which did not display a neurodegenerative phenotype. Taken together, this evidence suggests that the pathogenesis of p150^{glued}-associated diseases might be caused mainly by a gain-of-function effect [6,26].

Neurons of the hypoglossal nucleus and ventral horn in HMN7B and the substantia nigra and locus coeruleus in PS are substantially affected [1,2]. Although this means that neuronal cell lines are the most appropriate for studying the mechanisms that underlie the pathology of p150^{glued}-associated diseases, various studies have been performed using non-neuronal cell lines. For example, the CAP-Gly domain of p150^{glued} was needed for proper Golgi morphology in HeLa cells [10] and to activate cell division in Drosophila S2 cells [27]. G59S overexpression induced mitochondria-containing p150^{glued} aggregates and insufficient recovery of Golgi distribution following nocodazole treatment in COS7 cells. Overexpression of this mutant also increased cell death induction in MN1 mouse embryonic motor neuron cells [11]; however, this overexpression did not promote apoptosis induction by caspase-3 cleavage in COS7 cells or in rat primary motor neurons [28]. Although our data are from non-polarized and non-neuronal HeLa cells and thus might not reflect the precise physiological state of neurodegenerative disease, we believe that these results give us at least partial insight into the mechanisms underlying p150^{glued}-associated diseases. Further assessment with more appropriate cell lines, like neurons differentiated from induced pluripotent stem cells from the disease patients should be performed in the future.

Materials and Methods

Cell culture and transfection

HeLa and SH-SY5Y cells were maintained as previously described [29]. Cells were transfected using Lipofectamine 2000 (Invitrogen, Carlsbad, CA, USA) according to the manufacturer's protocols. For pharmacological studies, z-VAD-FMK (Calbiochem, San Diego, CA, USA, 219007), caspase-8 inhibitor II (Millipore, Billerica, MA, USA, 218759), and DMSO (Sigma, St.

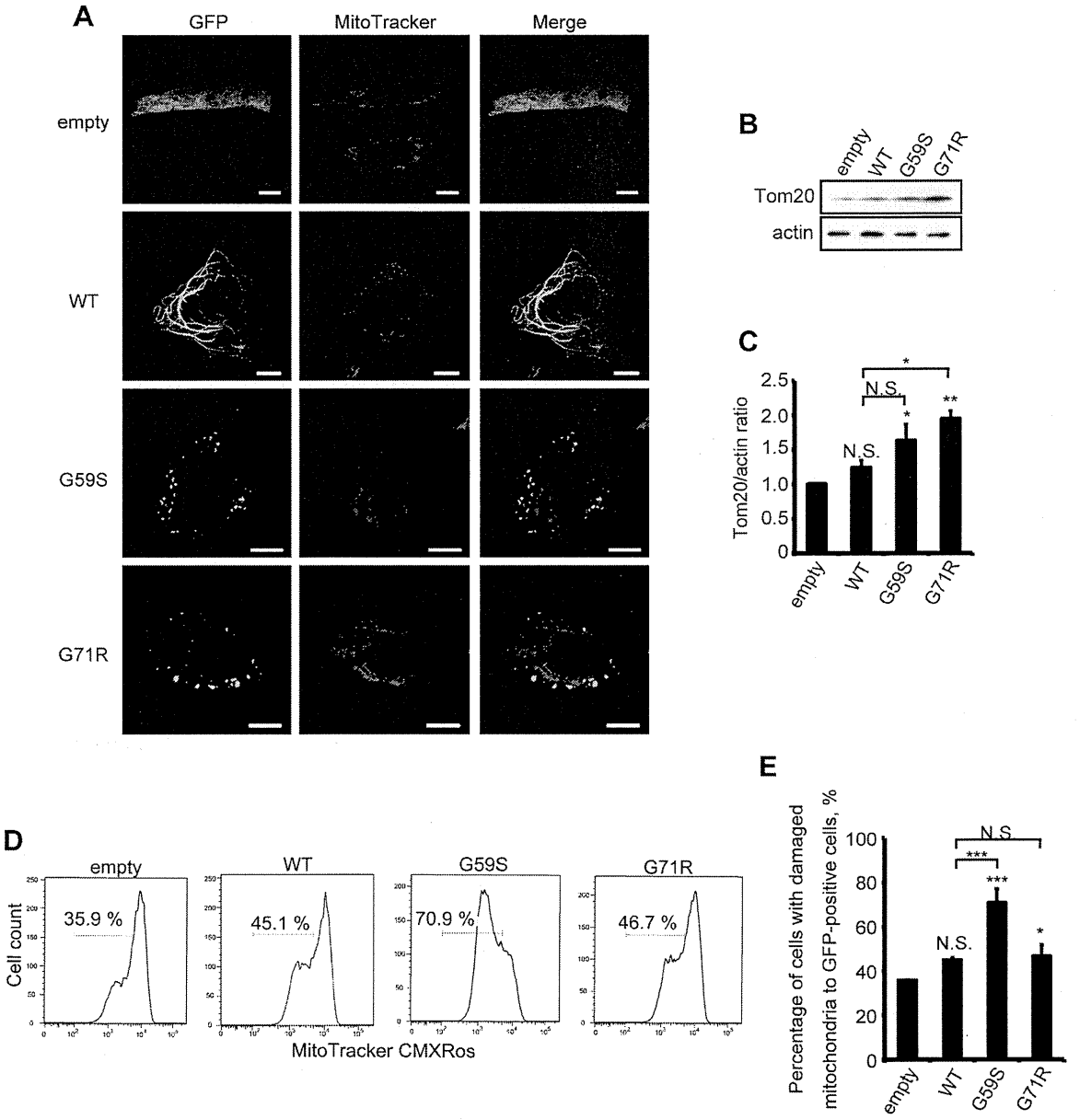

Figure 3. Abnormal mitochondria accumulate in cells overexpressing mutant p150^{glued}. (A) HeLa cells transfected with GFP-empty vector, GFP-tagged wild-type or mutant (G59S or G71R) p150^{glued} were incubated with MitoTracker Deep Red (100 nM) for 15 min and analyzed using confocal microscopy. Insets show higher magnification of the boxed areas. Bars, 10 μm. (B, C) Twenty-four hours after transfection, GFP-positive HeLa cells were sorted using flow cytometry and analyzed by immunoblotting with antibodies against TOM20 and actin (B). Densitometry analysis of TOM20 levels relative to actin was performed in three independent experiments (C). (D, E) Twenty-four hours after transfection, HeLa cells were incubated with Mitotracker-Red CMXRos (25 nM) for 15 min, and intracellular fluorescence intensity was measured by flow cytometry. The histograms of MitoTracker-Red CMXRos fluorescence in GFP-positive cells (D) and the percentages of GFP-positive cells with reduced mitochondrial potentials (E) are shown. The error bar indicates each standard deviation. Statistics are from three independent experiments: *, $p<0.05$; **, $p<0.01$; ***, $p<0.001$.

doi:10.1371/journal.pone.0094645.g003

Louis, MO, USA, D2650) were added at the indicated times and concentrations.

Plasmids

The wild-type *DCTN1* coding region was PCR-amplified from a cDNA plasmid kindly provided by Dr. Farrer MJ (University of British Columbia) using the following primers (Sigma): 5′-TCAAGGGAATTCAATGGCACAGAGCAAGAGGCAC-3′ and 5′-TCAAGGGATATCAGGGAGATGAGGCGACTGT-GAA-3′. The resulting fragment was inserted into the pFLAG-CMV5a vector (Sigma) using *Eco*RV and *Eco*RI. The plasmid was cut with *Eco*RI and *Kpn*I, and the insert was subcloned into pAcGFP-N3 (Clontech, Mountain View, CA, USA). Mutagenesis to create the six mutated p150^{glued} plasmids was performed using the Quikchange Lightning site-directed mutagenesis kit (Stratagene, La Jolla, CA, USA). The pCIneo-TDP43-FLAG plasmid

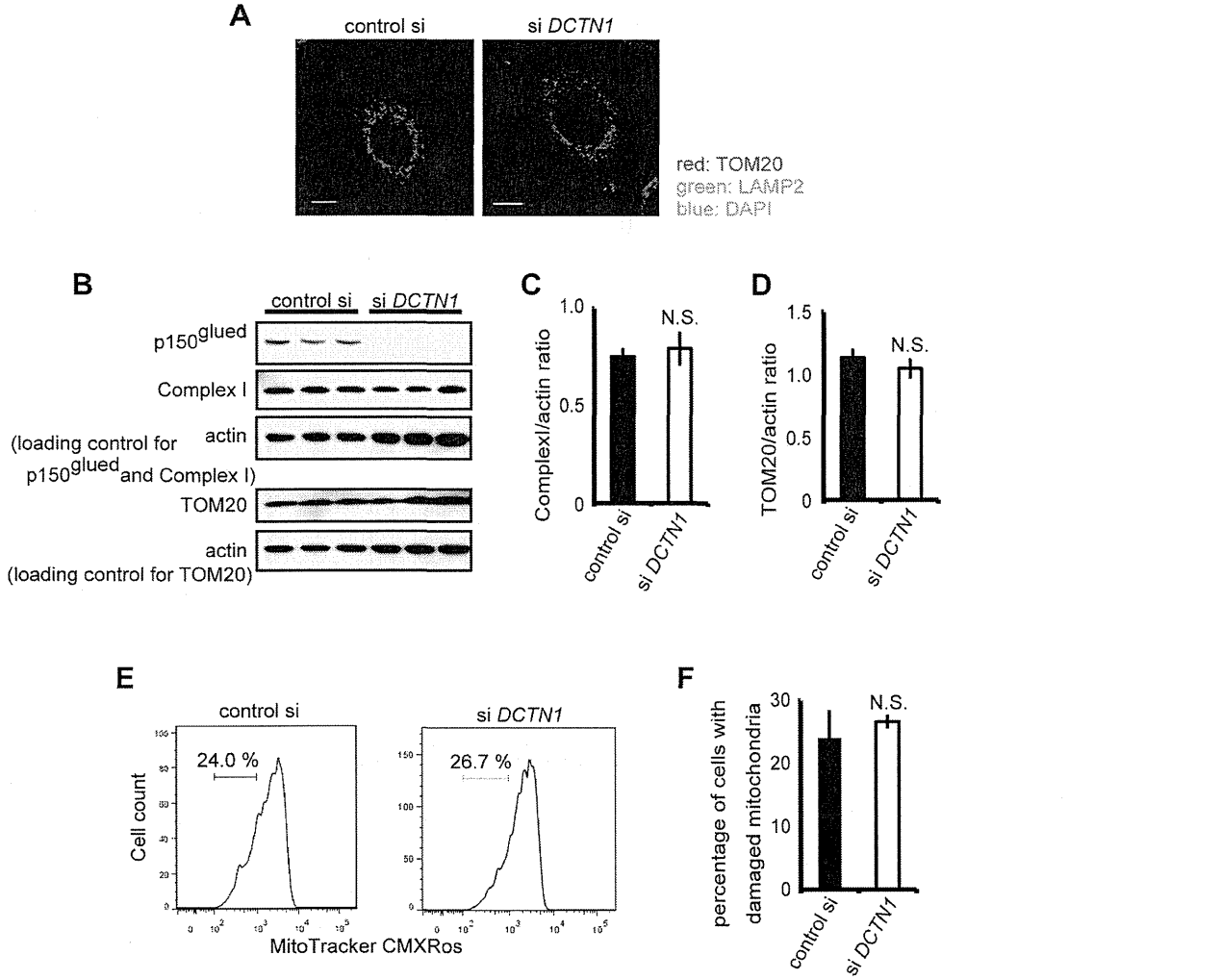

Figure 4. Depletion of p150^{glued} does not induce damaged mitochondria accumulation. (A) Control siRNA or DCTN1 siRNA transfected cells were fixed and co-stained with antibodies against LAMP2 (green) and TOM20 (red), and analyzed using confocal microscopy. Bars, 10 μm. (B) Control siRNA or DCTN1 siRNA transfected HeLa cells were analyzed by immunoblotting with antibodies against complex I, TOM20, and actin. (C, D) Densitometry analysis of complex I (C) and TOM20 (D) levels relative to actin was performed. (E, F) DCTN1 siRNA transfected HeLa cells were incubated with Mitotracker-Red CMXRos and intracellular fluorescence intensity was measured by flow cytometry. The histograms of MitoTracker-Red CMXRos fluorescence (E) and the percentages of cells with reduced mitochondrial potentials (F) are shown. The error bar indicates each standard deviation. Statistics are from three independent experiments: N.S., not significant.
doi:10.1371/journal.pone.0094645.g004

was kindly provided by Dr. Koji Yamanaka (RIKEN, Brain Science Institute, Wako, Japan).

RNA interference

CASP8, *CASP3*, and *DCTN1* siRNA were obtained as ON-TARGETplus *CASP8* siRNA SMARTpool (Dharmacon, Lafayette, CO, USA, L-003466-00), ON-TARGETplus *CASP3* siRNA SMARTpool (Dharmacon, L-004307-00), and ON-TARGETplus *DCTN1* siRNA (Dharmacon, J-012874-06), respectively. Non-targeting controls were also purchased from Dharmacon. Transfection of siRNA was performed using Lipofectamine 2000 according to the manufacturer's protocols (Invitrogen).

Immunocytochemistry

Cells were fixed with 4% paraformaldehyde (PFA) for 15 min, permeabilized with 50 μg/mL digitonin in 1 × phosphate-buffered saline (PBS) for 15 min, and incubated with 10% fetal bovine serum (FBS, Invitrogen) and 1% bovine serum albumin (BSA, Wako, Osaka, Japan) in 1 × PBS for 30 min at room temperature. Cells were then incubated overnight with primary antibodies at 4°C, followed by incubation with secondary antibodies for 1 h at room temperature. Cells were then mounted with Vectashield containing DAPI (Vector Laboratories, Burlingame, CA, USA). The following antibodies were used in this study: anti-FLAG (Sigma, F7425; 1:500), anti-α-tubulin (Sigma, T6199; 1:1000), anti-TOM20 (Santa Cruz Biotechnology, Santa Cruz, CA, USA, sc-11415; 1:500), and anti-cleaved caspase-3 (Cell Signaling Technology, Danvers, MA, USA, 9661; 1:800). Alexa Fluor 488- and 594-conjugated secondary antibodies (1:500) were from Invitrogen. For live-cell imaging, HeLa cells were grown on MatTek glass bottom dishes (MatTek Corp.) and transfected. After 24 hours, 200 nM MitoTracker Red CMXRos (Invitrogen) was added to the media for 15 min at 37°C, followed by a wash in PBS at 37°C. Images were acquired on a Zeiss LSM510 META

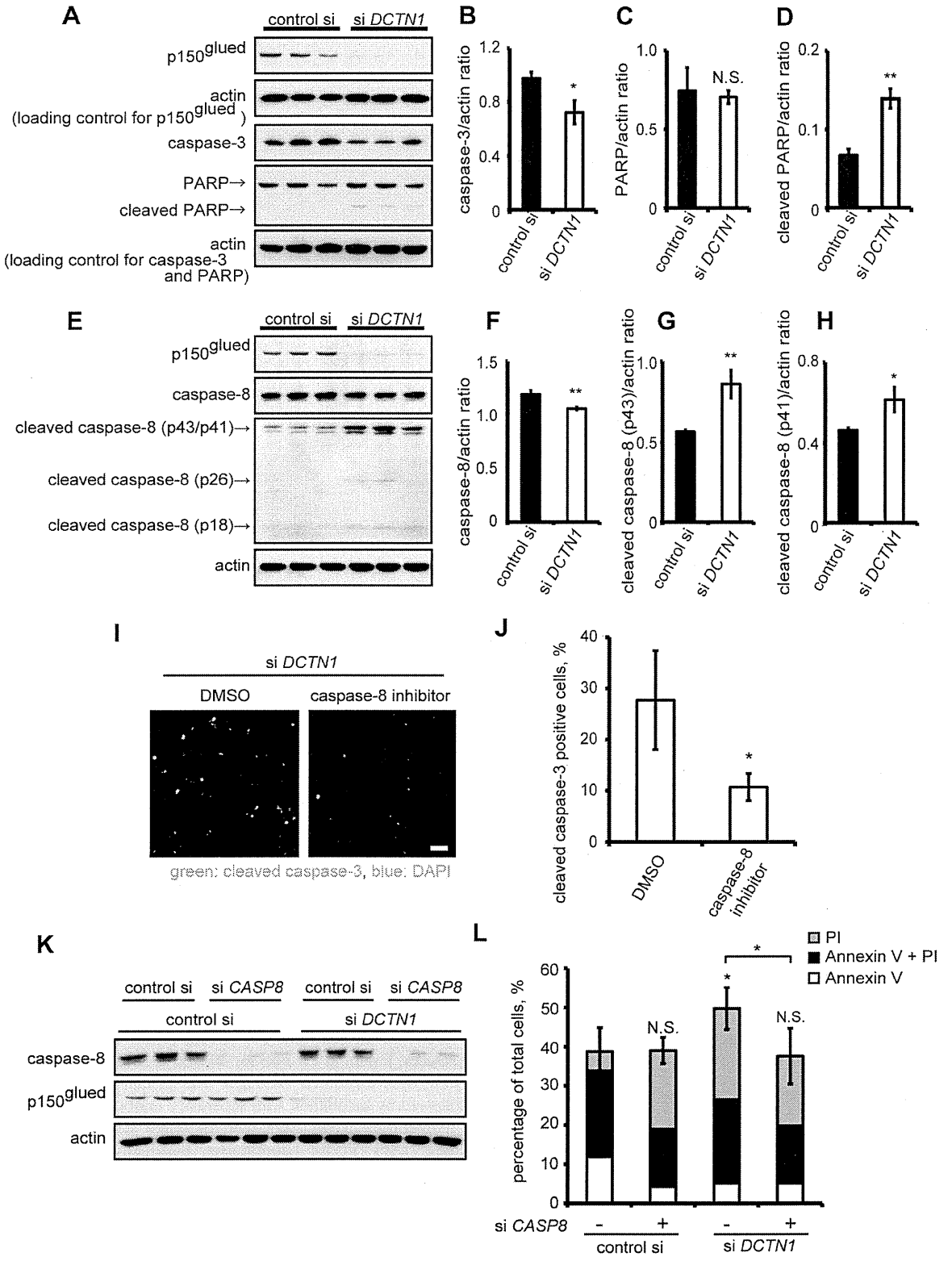

Figure 5. Depletion of p150glued activates apoptotic pathways via caspase-8 cleavage. (A–H) HeLa cells were transfected with control scrambled siRNA or DCTN1 siRNA for 72 h, and immunoblotting analysis was performed with antibodies against caspase-3, PARP, cleaved PARP, and actin (G), or caspase-8, cleaved caspase-8, and actin (E) to monitor the effects on the apoptotic pathway. Densitometry analysis of each protein levels relative to actin was performed (B–D, F–H). (I,J) HeLa cells were transfected with DCTN1 siRNA and incubated with DMSO or 25 μM caspase-8 inhibitor for 48 h. Cells were fixed and stained with antibodies to cleaved caspase-3 (green) and DAPI (blue), and analyzed using fluorescence microscopy (I). The percentage of cleaved caspase-3-positive cells is shown (J). Bars, 100 μm (K,L). Twenty-four hours after transfection with control scrambled siRNA

or CASP8 siRNA, HeLa cells were transfected with control or DCTN1 siRNA. Forty-eight hours after DCTN1 siRNA transfection, cells were analyzed by immunoblotting to monitor the knockdown efficiency of caspase-8 and p150^{glued} (K), and stained with Annexin V and PI to assess rates of cell death using flow cytometry (L). The error bar indicates each standard deviation. Statistics are from three independent experiments: N.S., not significant; *,p<0.05; **,p<0.01; ***,p<0.001.
doi:10.1371/journal.pone.0094645.g005

confocal microscope (Zeiss, Oberkochen, Germany) using a 63× water-immersion objective lens (NA = 1.2). Images were magnified using Zeiss LSM510 v3.2 software. Colocalization was quantified using the colocalization plugin of ImageJ 1.43 (NIH).

Quantification of aggregate formation and cleaved caspase-3 positive cells

Aggregate formation and cleaved caspase-3 positive cells were assessed using a fluorescence microscope (Axio Imager 2, Zeiss) with a 40× objective. GFP-positive or FLAG-positive cells were selected and the population of cells with aggregates was counted. Quantification was based on at least three independent experiments, each carried out in triplicate, and 100–300 cells were counted in each slide. The scorer was blinded to the identity of the slides.

Cell viability assays

GFP-positive cells were scored 24 and 48 h after transfection for abnormal cell nuclei, according to previously reported criteria [30] using a fluorescence microscope (Axio Imager 2) with a 40× objective. Analysis was performed with at least three independent experiments, each carried out in triplicate, and 100–400 cells were counted on each slide. The scorer was blinded to the identity of the slides. Detection of apoptotic cells was also determined using an annexin V/propidium iodide (PI) detection kit (Invitrogen), according to the manufacturer's protocol. Briefly, cells were harvested and washed with 1× PBS 24 and 48 h after transfection. They were then incubated at room temperature with annexin V/Alexa350 and PI for 15 min and analyzed by flow cytometry (LSRFortessa, BD Biosciences, San Jose, CA, USA).

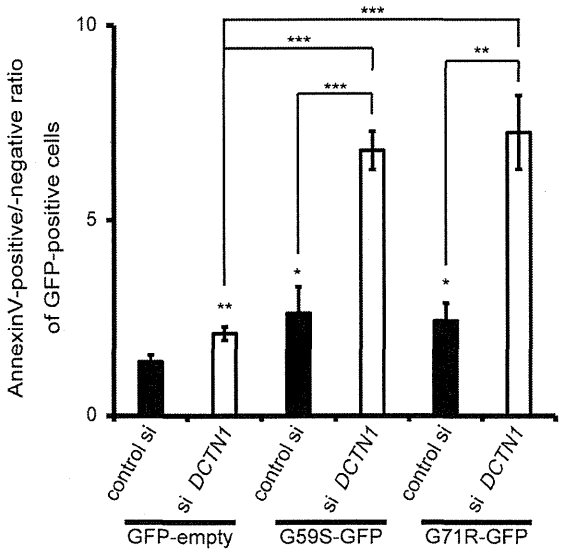

Figure 6. Depletion of p150^{glued} accelerates mutant p150^{glued}-induced cell death. Forty-eight hours after transfection with control scrambled siRNA or DCTN1 siRNA, HeLa cells were transfected with GFP-empty vector or mutant (G59S or G71R) p150^{glued} for 24 h. Cells were stained with Annexin V, and GFP-positive cells were analyzed by flow cytometry. The ratios of Annexin V-positive cells relative to Annexin V-negative cells were calculated. The error bar indicates each standard deviation. Statistics are from three independent experiments: *,p<0.05; **,p<0.01; ***,p<0.001.
doi:10.1371/journal.pone.0094645.g006

Flow cytometry analysis

Changes in the mitochondrial membrane potentials were assessed with MitoTracker Red CMXRos (Invitrogen). Twenty-four hours after transfection, PBS-washed cells were incubated in 50 nM MitoTracker Red CMXRos for 15 min at 37°C. After washing, cells were suspended in 1× PBS and were analyzed by flow cytometry.

Cleaved caspase-3 labeling was performed according to the flow cytometry protocol from Cell Signaling Technology. Briefly, HeLa cells were pelleted 24 h after transfection, fixed in 4% PFA for 10 min at 37°C and for 1 min on ice. The samples were permeabilized with ice-cold 90% methanol for 30 min on ice and then were blocked in 100 µL of incubation buffer (0.5 g BSA in 100 ml PBS) for 10 min at room temperature. Labeling of the samples was performed with anti-cleaved caspase-3 (Cell Signaling Technology, 9661; 1:800) antibodies for 1 h at room temperature. After incubation, the samples were washed and resuspended in incubation buffer containing Alexa 647-conjugated secondary antibody (Invitrogen-Molecular Probes; 1:500) for 30 min at room temperature. The samples were washed, resuspended in PBS and analyzed by flow cytometry. For flow cytometry analysis, 2,000–5,000 GFP-positive cells were analyzed for each sample and the experiments were performed at least in triplicate. Data were analyzed with CellQuest (BD Biosciences) and FlowJo software (Tree Star Inc., Ashland, OR, USA).

Western blotting

Cells transfected with *DCTN1* siRNA or GFP-tagged vectors for indicated times were lysed in cold RIPA buffer [25 mM Tris-HCl pH 7.6, 150 mM NaCl, 1% NP-40, 1% sodium deoxycholate, 0.1% sodium dodecyl sulfate (SDS)] in the presence of protease inhibitors (Roche, Basel, Switzerland) for 20 min on ice. The lysates were centrifuged and the resulting supernatants mixed in NuPAGE LDS sample buffer (Invitrogen). The samples were resolved on 10–20% Tris-HCl gels (Bio Craft, Agra, India, MDG-297) in 1× Tris/Glycine/SDS buffer (Bio-Rad, Hercules, CA, USA) and transferred onto polyvinylidene fluoride (PVDF) membrane (Millipore). The membranes were blocked for 1 h in Tris-buffered saline (TBS) containing 0.05% Tween-20 (TBS-T) and 5% non-fat milk (BD Difco) and then incubated overnight at 4°C with the primary antibody. The membranes were washed with PBS-T three times followed by incubation for 1 h at room temperature with horseradish peroxidase-conjugated anti-mouse, rabbit, and guinea pig IgG (GE Health Care Biosciences, Pittsburgh, PA, USA). Immunoreactivity was assessed by chemiluminescence reaction using the ECL prime reagent (GE Health Care Biosciences). The antibodies used were as follows: anti-actin (Millipore, clone C4; 1:10000), anti-p150^{glued} (BD, 610473; 1:5000), anti-TOM20 (Santa Cruz, sc-11415; 1:1000), anti-complex I (Invitrogen, 459100; 1:1000), anti-caspase-3 (Cell Signaling Technology, 9665; 1:1000), anti-PARP (Cell Signaling Technology, 9542; 1:1000), anti-caspase-8 (Cell Signaling Tech-

nology, 4790; 1:500), and anti-cleaved caspase-8 (Cell Signaling Technology, 9496; 1:1000).

Electron microscopy

HeLa cells were plated on Thermanox plastic coverslips (Nunc, Penfield, NY, USA) and transfected with pAcGFP-empty, wild-type, G59S, and G71R p150^{glued} plasmids. Twenty-four hours after transfection, one set of cells was pre-fixed in 2% glutaraldehyde in 0.1 M phosphate buffer (pH 7.4) at 4°C, and post-fixed with 2% OsO_4 in phosphate buffer for 1 h at 4°C. After fixation, they were dehydrated in a graded series of ethanol, placed in propylene oxide, and embedded in epoxy resin (Quetol 812, Nisshin-EM, Tokyo, Japan). Ultra-thin sections (90–100 nm) were cut using an ULTRACUT-UCT (Leica, Wetzlar, Germany) with a diamond knife. Sections were stained with 2% uranyl acetate in distilled water for 15 min followed by a lead staining solution for 5 min.

For immune electron microscopic analysis, another set of cells was pre-fixed in 4% PFA and 0.1% glutaraldehyde in phosphate buffer at 4°C, and post-fixed with 1% OsO_4 and 1.5% potassium ferricyanide in phosphate buffer for 1 h at 4°C. After fixation, they were dehydrated in a graded series of ethanol and embedded in LR White resin. Ultra-thin sections were cut, and samples were incubated in 3.8% sodium periodate for 1 h at room temperature. Samples were blocked with 2% BSA in PBS for 30 min at room temperature and then immunolabeled with primary anti-GFP antibody (Living Colors A.v. Peptide Antibody, Clontech, 632377; 1:10) followed by anti-rabbit immunogold (BB International, Cardiff, UK; 1:100). Afterwards, these samples were stained with 2% uranyl acetate in distilled water for 5 min followed by a lead staining solution for 1 min. All sections were examined with a JEM-1200EX (JEOL, Peabody, MA, USA) electron microscope at 80 KV.

Statistical analysis

Densitometry analysis was performed on immunoblots from three independent experiments using ImageJ 1.43. Differences among means were analyzed using 1- or 2-way ANOVA, followed, when results showed significant differences, by pair-wise comparisons between means using Tukey's Honestly Significant Difference Test. When only two groups were compared, the Student's t test was used. In all analyses, the null hypothesis was rejected at the 0.05 level. SYSTAT 13 software (Hulinks, Tokyo, Japan) was used for statistical calculations.

Supporting Information

Figure S1 Overexpression of mutant p150^{glued} disrupts p150^{glued} distribution and causes aggregate formation. (A) HeLa cells transfected with GFP-tagged wild-type or mutant p150^{glued} were fixed after 24 h and analyzed using confocal microscopy. Bars, 10 μm. (B) SH-SY5Y cells transfected with GFP-tagged wild-type or mutant (G59S or G71R) p150^{glued} were fixed and stained with an antibody against α-tubulin (red) after 24 h and analyzed using confocal microscopy. Bars, 10 μm. (C) HeLa cells transfected with 3xFLAG-tagged wild-type or mutant p150^{glued} were fixed and co-stained with antibodies against FLAG (green) and α-tubulin (red) after 24 h. Bars, 10 μm. (D) FLAG-positive cells were counted from three independent experiments. The percentage of FLAG-positive cells with aggregates is shown. The error bar indicates each standard deviation. Statistics are from three independent experiments. (E) Electron microscopy examination of HeLa cells transfected with GFP-tagged G59S or G71R p150^{glued}. Images on the right are magnified images of the boxed area from the left. Intracytoplasmic aggregate (a) is labeled. (F) HeLa cells were transfected with GFP-tagged wild-type or mutant (G59S or G71R) p150^{glued}, and cells were fixed and stained with anti-polyubiquitin antibody (FK2) after 24 h. (G) HeLa cells were co-transfected with FLAG-tagged TDP-43 and GFP-tagged wild-type or mutant (G59S or G71R) p150^{glued}, and cells were fixed and stained with antibody against FLAG after 24 h. Bars, 10 μm.
(TIF)

Figure S2 Mutant p150^{glued}-dependent apoptosis is not blocked by caspase-8 siRNA knockdown. (A, B) HeLa cells were transfected with control scrambled siRNA or caspase-8 siRNA for 72 h, and immunoblotting analyses were performed to monitor the knockdown efficiency of caspase-8 siRNA (A). Densitometry analysis of caspase-8 levels relative to actin was performed (B). (C, D). Twenty-four hours after transfection with control siRNA or caspase-8 siRNA, HeLa cells were transfected with GFP-empty or GFP-tagged G59S p150^{glued}. Forty-eight hours after transfection, cells were stained with Annexin V and PI, and GFP-positive cells were analyzed by flow cytometry. The error bar indicates each standard deviation. Statistics are from three independent experiments: N.S., not significant; ***,$p<0.001$.
(TIF)

Acknowledgments

We thank Drs. Takashi Ueno (Department of Biochemistry, Juntendo University) and Shigeto Sato (Department of Neurology, Juntendo University) for critical comments. We also thank Drs. Koji Yamanaka (RIKEN, Brain Science Institute) and Matthew J. Farrer (University of British Columbia) for providing us with plasmids.

Author Contributions

Conceived and designed the experiments: KI SS NF SK YT NH. Performed the experiments: KI SS YI HS. Analyzed the data: KI SS DY. Contributed reagents/materials/analysis tools: KI SS NF YL MK. Wrote the paper: KI SS NF.

References

1. Wider C, Wszolek ZK (2008) Rapidly progressive familial parkinsonism with central hypoventilation, depression and weight loss (Perry syndrome)—a literature review. Parkinsonism Relat Disord 14: 1–7.
2. Puls I, Jonnakuty C, LaMonte BH, Holzbaur EL, Tokito M, et al. (2003) Mutant dynactin in motor neuron disease. Nat Genet 33: 455–456.
3. Lloyd TE, Machamer J, O'Hara K, Kim JH, Collins SE, et al. (2012) The p150(Glued) CAP-Gly domain regulates initiation of retrograde transport at synaptic termini. Neuron 74: 344–360.
4. Moughamian AJ, Holzbaur EL (2012) Dynactin is required for transport initiation from the distal axon. Neuron 74: 331–343.
5. Chevalier-Larsen ES, Wallace KE, Pennise CR, Holzbaur EL (2008) Lysosomal proliferation and distal degeneration in motor neurons expressing the G59S mutation in the p150Glued subunit of dynactin. Hum Mol Genet 17: 1946–1955.
6. Lai C, Lin X, Chandran J, Shim H, Yang WJ, et al. (2007) The G59S mutation in p150(glued) causes dysfunction of dynactin in mice. J Neurosci 27: 13982–13990.
7. Laird FM, Farah MH, Ackerley S, Hoke A, Maragakis N, et al. (2008) Motor neuron disease occurring in a mutant dynactin mouse model is characterized by defects in vesicular trafficking. J Neurosci 28: 1997–2005.
8. Farrer MJ, Hulihan MM, Kachergus JM, Dachsel JC, Stoessl AJ, et al. (2009) DCTN1 mutations in Perry syndrome. Nat Genet 41: 163–165.
9. Lazarus JE, Moughamian AJ, Tokito MK, Holzbaur EL (2013) Dynactin subunit p150(Glued) is a neuron-specific anti-catastrophe factor. PLoS Biol 11: e1001611.
10. Dixit R, Levy JR, Tokito M, Ligon LA, Holzbaur EL (2008) Regulation of dynactin through the differential expression of p150Glued isoforms. J Biol Chem 283: 33611–33619.

11. Levy JR, Sumner CJ, Caviston JP, Tokito MK, Ranganathan S, et al. (2006) A motor neuron disease-associated mutation in p150Glued perturbs dynactin function and induces protein aggregation. J Cell Biol 172: 733–745.
12. Sarkar S, Krishna G, Imarisio S, Saiki S, O'Kane CJ, et al. (2008) A rational mechanism for combination treatment of Huntington's disease using lithium and rapamycin. Hum Mol Genet 17: 170–178.
13. McCarthy NJ, Whyte MK, Gilbert CS, Evan GI (1997) Inhibition of Ced-3/ICE-related proteases does not prevent cell death induced by oncogenes, DNA damage, or the Bcl-2 homologue Bak. J Cell Biol 136: 215–227.
14. Kawajiri S, Saiki S, Sato S, Sato F, Hatano T, et al. (2010) PINK1 is recruited to mitochondria with parkin and associates with LC3 in mitophagy. FEBS Lett 584: 1073–1079.
15. Yoshii SR, Kishi C, Ishihara N, Mizushima N (2011) Parkin mediates proteasome-dependent protein degradation and rupture of the outer mitochondrial membrane. J Biol Chem 286: 19630–19640.
16. Geisler S, Holmstrom KM, Skujat D, Fiesel FC, Rothfuss OC, et al. (2010) PINK1/Parkin-mediated mitophagy is dependent on VDAC1 and p62/SQSTM1. Nat Cell Biol 12: 119–131.
17. Morlino G, Barreiro O, Baixauli F, Robles-Valero J, Gonzalez-Granado JM, et al. (2014) Miro-1 links mitochondria and microtubule dynein motors to control lymphocyte migration and polarity. Mol Cell Biol.
18. van Spronsen M, Mikhaylova M, Lipka J, Schlager MA, van den Heuvel DJ, et al. (2013) TRAK/Milton motor-adaptor proteins steer mitochondrial trafficking to axons and dendrites. Neuron 77: 485–502.
19. van der Bliek AM, Shen Q, Kawajiri S (2013) Mechanisms of mitochondrial fission and fusion. Cold Spring Harb Perspect Biol 5.
20. Schwarz TL (2013) Mitochondrial trafficking in neurons. Cold Spring Harb Perspect Biol 5.
21. Pilling AD, Horiuchi D, Lively CM, Saxton WM (2006) Kinesin-1 and Dynein are the primary motors for fast transport of mitochondria in Drosophila motor axons. Mol Biol Cell 17: 2057–2068.
22. Varadi A, Johnson-Cadwell LI, Cirulli V, Yoon Y, Allan VJ, et al. (2004) Cytoplasmic dynein regulates the subcellular distribution of mitochondria by controlling the recruitment of the fission factor dynamin-related protein-1. J Cell Sci 117: 4389–4400.
23. Jucker M, Walker LC (2013) Self-propagation of pathogenic protein aggregates in neurodegenerative diseases. Nature 501: 45–51.
24. Fujiwara T, Morimoto K (2012) Cooperative effect of p150Glued and microtubule stabilization to suppress excitotoxicity-induced axon degeneration. Biochem Biophys Res Commun 424: 82–88.
25. Fujiwara T, Morimoto K, Kakita A, Takahashi H (2012) Dynein and dynactin components modulate neurodegeneration induced by excitotoxicity. J Neurochem 122: 162–174.
26. Lipka J, Kuijpers M, Jaworski J, Hoogenraad CC (2013) Mutations in cytoplasmic dynein and its regulators cause malformations of cortical development and neurodegenerative diseases. Biochem Soc Trans 41: 1605–1612.
27. Kim H, Ling SC, Rogers GC, Kural C, Selvin PR, et al. (2007) Microtubule binding by dynactin is required for microtubule organization but not cargo transport. J Cell Biol 176: 641–651.
28. Stockmann M, Meyer-Ohlendorf M, Achberger K, Putz S, Demestre M, et al. (2013) The dynactin p150 subunit: cell biology studies of sequence changes found in ALS/MND and Parkinsonian syndromes. J Neural Transm 120: 785–798.
29. Saiki S, Sasazawa Y, Imamichi Y, Kawajiri S, Fujimaki T, et al. (2011) Caffeine induces apoptosis by enhancement of autophagy via PI3K/Akt/*m*TOR/p70S6K inhibition. Autophagy 7: 176–187.
30. Ravikumar B, Duden R, Rubinsztein DC (2002) Aggregate-prone proteins with polyglutamine and polyalanine expansions are degraded by autophagy. Hum Mol Genet 11: 1107–1117.

BASIC RESEARCH PAPER

Autophagy 10:4, 1–11; April 2014; © 2014 Landes Bioscience

PARK2/Parkin-mediated mitochondrial clearance contributes to proteasome activation during slow-twitch muscle atrophy via NFE2L1 nuclear translocation

Norihiko Furuya,[1,†,‡,*] Shin-Ichi Ikeda,[2] Shigeto Sato,[3] Sanae Soma,[1] Junji Ezaki, [1] Juan Alejandro Oliva Trejo,[1] Mitsue Takeda-Ezaki,[1] Tsutomu Fujimura,[4] Eri Arikawa-Hirasawa,[3,5] Norihiro Tada,[5] Masaaki Komatsu,[6] Keiji Tanaka,[7] Eiki Kominami,[1] Nobutaka Hattori,[3] and Takashi Ueno[1,§,*]

[1]Department of Biochemistry; Juntendo University School of Medicine; Bunkyo-ku, Tokyo Japan; [2]Sportology Center; Juntendo University Graduate School of Medicine; Bunkyo-ku, Tokyo Japan; [3]Department of Neurology; Juntendo University School of Medicine; Bunkyo-ku, Tokyo Japan; [4]Laboratory of Proteomics and Biomolecular Science; Research Support Center; Juntendo University Graduate School of Medicine; Bunkyo-ku, Tokyo Japan; [5]Research Institute for Diseases of Old Age; Juntendo University Graduate School of Medicine; Bunkyo-ku, Tokyo Japan; [6]Protein Metabolism Project; Tokyo Metropolitan Institute of Medical Science; Setagaya-ku, Tokyo Japan; [7]Laboratory of Protein Metabolism; Tokyo Metropolitan Institute of Medical Science; Setagaya-ku, Tokyo Japan

Current affiliation: [†]Department of Research and Therapeutics for Movement Disorders; Juntendo University Graduate School of Medicine; Bunkyo-ku, Tokyo Japan; [‡]Department of Neurology; Juntendo University School of Medicine; Bunkyo-ku, Tokyo Japan; [§]Laboratory of Proteomics and Biomolecular Science; Research Support Center; Juntendo University Graduate School of Medicine; Bunkyo-ku, Tokyo Japan

Keywords: PARK2-mediated mitophagy, skeletal muscle atrophy, proteasome, NFE2L1, slow-twitch muscle, autophagy, mitochondria, knockout mouse

Abbreviations: ARE, antioxidant response element; CCCP, carbonyl cyanide m-chlorophenylhydrazone; NAC, N-acetyl-cysteine; NFE2L1, nuclear factor erythroid-derived 2-related factor 1; NFE2L2, nuclear factor erythroid-derived 2-related factor 2; ROS, reactive oxygen species; tBHQ, tert-butyl hydroquinone

Skeletal muscle atrophy is thought to result from hyperactivation of intracellular protein degradation pathways, including autophagy and the ubiquitin–proteasome system. However, the precise contributions of these pathways to muscle atrophy are unclear. Here, we show that an autophagy deficiency in denervated slow-twitch soleus muscles delayed skeletal muscle atrophy, reduced mitochondrial activity, and induced oxidative stress and accumulation of PARK2/Parkin, which participates in mitochondrial quality control (PARK2-mediated mitophagy), in mitochondria. Soleus muscles from denervated *Park2* knockout mice also showed resistance to denervation, reduced mitochondrial activities, and increased oxidative stress. In both autophagy-deficient and *Park2*-deficient soleus muscles, denervation caused the accumulation of polyubiquitinated proteins. Denervation induced proteasomal activation via NFE2L1 nuclear translocation in control mice, whereas it had little effect in autophagy-deficient and *Park2*-deficient mice. These results suggest that PARK2-mediated mitophagy plays an essential role in the activation of proteasomes during denervation atrophy in slow-twitch muscles.

Introduction

Skeletal muscles occupy up to 55% of total body mass in mammals, and generate motile forces and heat. They are a major site for carbohydrate and fatty acid metabolism and are categorized into 2 types exhibiting distinct contractile and metabolic properties: slow-twitch, oxidative fatigue-resistant muscles and fast-twitch, glycolytic fatigue-susceptible muscles. The slow-twitch muscle fibers typically display a 2- to 3-fold higher mitochondrial density and substantially lower capacity for nonoxidative ATP synthesis compared with the fast-twitch muscle fibers.

Maintenance of muscle mass depends on a balance between protein synthesis and degradation. Innervation of skeletal muscle fibers by motor neurons is essential for maintenance of muscle size, structure, and function. Numerous disorders, including amyotrophic lateral sclerosis, Guillain-Barre syndrome, polio, and polyneuropathy, disrupt the nerve supply to muscle, causing

*Correspondence to: Norihiko Furuya; Email: nohuruya@juntendo.ac.jp; Takashi Ueno; Email: upfield@juntendo.ac.jp
Submitted: 08/20/2013; Revised: 01/06/2014; Accepted: 01/09/2014
http://dx.doi.org/10.4161/auto.27785

©2014 Landes Bioscience. Do not distribute.

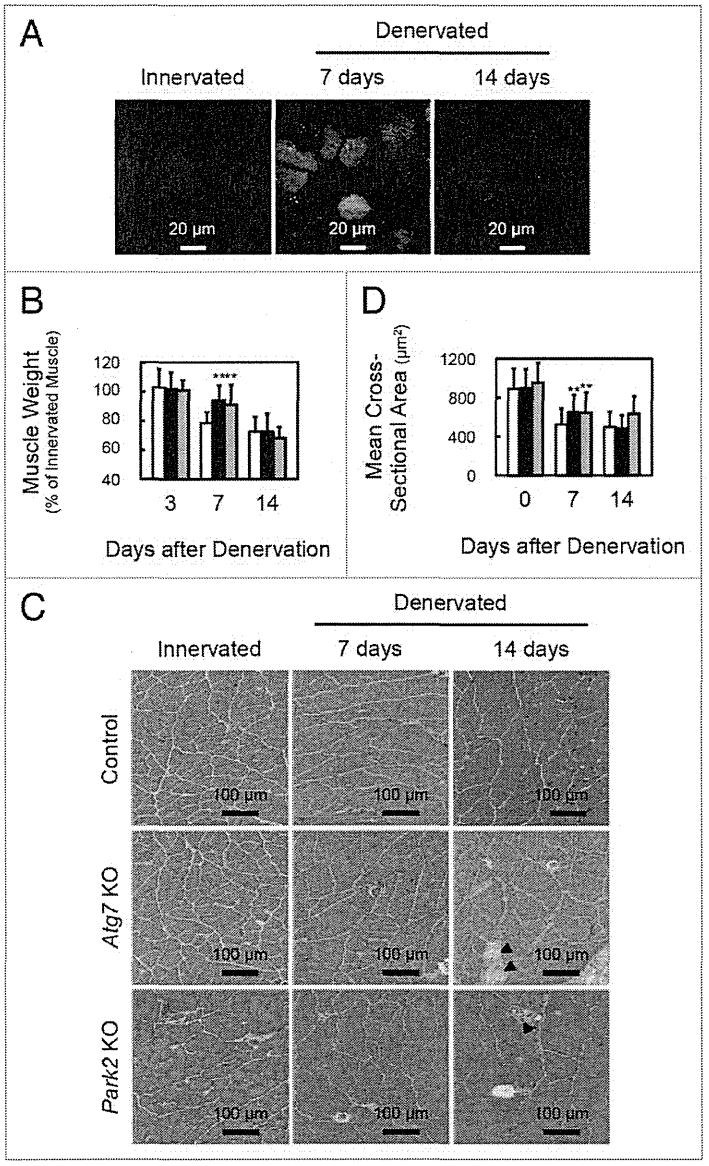

Figure 1. Delay of denervation atrophy in autophagy-deficient and PARK2-deficient soleus muscle. (**A**) Representative images of soleus muscles from GFP-LC3 transgenic mice at 0 (innervated), 7 and 14 d after denervation. Scale bar, 20 μm. (**B**) Time course of weight loss in the soleus muscles of denervated mice. For the denervation procedure, the left sciatic nerves of control mice (open bar: day 3, n = 9; day 7, n = 28; day 14, n = 19), *Atg7* KO mice (closed bar: day 3, n = 12; day 7, n = 30; day 14, n = 14) or *Park2* KO mice (gray bar: day 3, n = 3; day 7, n = 13; day 14, n = 7) were cut in the mid-thigh region, leading to denervation of the lower limb muscles. Denervated muscle weight data are shown as the percentage of the weight of the contralateral innervated muscle from the right limb. Data are shown as the means ± s.d. $^{**}P < 0.01$ vs control mice at the same time. (**C**) Histological analysis of control, *Atg7* KO and *Park2* KO soleus muscles. Cryosections were stained with hematoxylin and eosin. Arrowheads, dead myofibers. Scale Bars: 100 μm. (**D**) Quantification of the cross-sectional areas of myofibers. Values are the means ± s.d. vs control mice at the same time, $^{**}P < 0.01$.

loss of muscle mass strength and endurance (referred to as neurogenic atrophy).[1,2] Other pathological states and systemic disorders, including cancer, diabetes, fasting, sepsis, and disuse, also cause muscle atrophy. The resulting loss of muscle mass in these conditions involves an activation of intracellular protein degradation and a decrease in protein synthesis. The ubiquitin-proteasome system (UPS) and autophagy are the 2 major pathways leading to intracellular degradation, and, when upregulated by the activation of FOXO transcription factors, both systems can contribute to skeletal muscle atrophy.[3-6]

The UPS is responsible for biologically important cellular processes including cell cycle progression, DNA repair, signaling cascades, cell death, immunity, developmental programs, and protein quality control by catalyzing selective degradation of regulatory proteins and damaged proteins.[7,8] Macroautophagy (hereafter referred to as autophagy) is a membrane dynamic process in which cytoplasmic components including macromolecules and organelles are sequestered into double-membrane structures called autophagosomes and delivered to lysosomes for degradation.[9,10] Autophagy participates not only in supplying amino acids under nutrient-poor environments, but also in the clearance of misfolded or aggregated proteins, damaged organelles, and pathogens. Currently, the differences between the contributions of the UPS and autophagy to the process of muscle atrophy are not clear.

Results

Autophagy is required for the early steps of denervation atrophy in soleus muscle

To ascertain whether autophagy is activated in atrophying muscles, we subjected GFP-LC3 transgenic mice[11] to denervation of the sciatic nerve, a model of skeletal muscle atrophy (**Fig. 1A**; **Fig. S1A**). Many GFP-LC3 puncta were observed in both slow-twitch soleus muscles and fast-twitch plantaris muscles of mice at 7 and 14 d after denervation. In the initial stage (within 48 h) of denervation atrophy, autophagy is suppressed by the proteasome-dependent MTORC1 activation.[12] However, these results show that autophagy is activated in atrophying hind-limb muscles. As previously reported, autophagy deficiency in skeletal muscle causes more muscle loss owing to denervation than occurs in the control situation with normal autophagy, and autophagy is required to maintain muscle mass.[4] However the contribution of autophagy to the process of muscle atrophy is not clear. We generated mice with a skeletal muscle-specific *Atg7* (an essential gene for autophagy) knockout under the control of the tamoxifen-inducible human skeletal actin (HSA) promoter ($Atg7^{Flox/Flox}$: HSA-Cre-ER^{T2}, hereinafter referred to as *Atg7* KO mice), and subjected them to denervation. The plantaris muscles, a fast-twitch glycolytic skeletal muscle, from both *Atg7* KO and control ($Atg7^{Flox/Flox}$) mice, were atrophied to almost the same extent by denervation (**Fig. S1B**). In contrast, the soleus muscle, a slow-twitch oxidative skeletal muscle, from *Atg7* KO

©2014 Landes Bioscience. Do not distribute.

mice, showed resistance to denervation at 7 d after denervation (**Fig. 1B–D**; **Fig. S2A**). However, the soleus muscles from *Atg7* KO mice and control mice exhibited comparable muscle mass and myofiber size at 14 d after denervation. Notably, dead myofibers were frequently observed in the *Atg7* KO soleus muscles at 14 d (**Fig. 1C**). The enhanced cell death at 14 d most likely contributes to the shrinking of the soleus muscle of *Atg7* KO mice. The phenotypes of soleus muscles of *Atg7* KO mice at 14 d after denervation are coincident with the previous study.[4] However, the phenotypes at a period earlier than 14 d after denervation were not investigated in that study. Thus, our finding seemed to reflect a more direct effect of autophagy-deficiency on muscle atrophy. These results indicated that autophagy contributes to the early stage of denervation atrophy and that autophagy deficiency delays atrophy in soleus muscle. In contrast, autophagy in fast-twitch muscles seems not to play an important role in the early stage of denervation atrophy, in spite of its activation by denervation in GFP-LC mice.

Denervated soleus muscle from *Atg7* KO mice shows mitochondrial dysfunction

To elucidate the precise phenotypes of the soleus muscles of denervated *Atg7* KO mice at 7 d after denervation, histological analyses were performed (**Fig. 2A**). The ratio of type I to type II muscle fibers in both innervated and denervated soleus muscles was almost the same in control and *Atg7* KO mice. Meanwhile, denervated soleus muscles from *Atg7* KO mice exhibited reduced staining for succinate dehydrogenase (SDH; complex II) and cytochrome *c* oxidase (Cox; complex IV) compared with denervated soleus muscles from control mice (**Fig. 2A and B**), indicating that the respiratory chain activities of denervated soleus muscles of *Atg7* KO mice were significantly decreased. The reduction of respiratory chain activities was not observed in denervated plantaris muscles from *Atg7* KO mice (**Fig. S1D**). As frequently reported for other autophagy-deficient mice, electron microscopy analysis revealed that abnormally swollen mitochondria were observed in the soleus muscles of denervated *Atg7* KO mice (**Fig. 2C**),[13-16] whereas, most of the mitochondria were morphologically normal in the soleus muscles of denervated *Atg7* KO mice. As was the case in GFP-LC3 mice, denervation induced formation of autophagic vacuoles (AVs) in the soleus muscles of control mice, whereas AVs were rarely observed in denervated soleus muscles of *Atg7* KO mice (**Fig. 2C**). These results indicated that autophagy deficiency leads to abnormal accumulation of mitochondria in the denervated soleus muscles. However, the expression levels of marker proteins for the outer membrane (e.g., TOMM20/Tom20), the intermembrane space (e.g., CYCS/cytochrome *c*), the inner membrane (e.g., OPA1), and the matrix (e.g., PDHA1/pyruvate dehydrogenase α1;) of mitochondria, and PPARGC1A/PGC1α, a master regulator of mitochondrial biogenesis, in denervated soleus muscles from *Atg7* KO mice, were comparable to those in the denervated muscles of control mice (**Fig. 2D**; **Fig. S2B**). The expression levels of DNM1L/Drp1 and FIS1/Fis1, which promote the fragmentation of mitochondria (Romanello et al., 2010), were not influenced by denervation. Mitochondrial DNA (mtDNA) copy numbers in denervated *Atg7* KO soleus muscles were not different from those in denervated control soleus muscles (**Fig. 2E**; **Fig. S2C**). Taken together, these results indicate that the decreased respiratory chain activities of denervated *Atg7* KO soleus muscle can be attributed to a qualitative reduction in mitochondrial function, but not to a decreased quantity of mitochondria. It is important to clarify the reason for the reduced mitochondrial function in denervated *Atg7* KO soleus muscles. Generally, oxidative stress is inseparably associated with dysregulation or disruption of mitochondrial functions, because mitochondria are both generators and targets of reactive oxygen species (ROS).[17] To ascertain whether ROS accumulate in denervated *Atg7* KO soleus muscles, we performed immunostaining with an antibody against 8-hydroxydeoxyguanosine (8-OHdG), a marker of ROS (**Fig. S3**). The denervated *Atg7* KO soleus muscles accumulated much more 8-OHdG than did the denervated control or the innervated *Atg7* KO soleus muscles. Moreover, the accumulation of carbonylated proteins was greater in denervated *Atg* KO soleus muscles than in denervated control or innervated *Atg7* KO muscles (**Fig. 2D**). These results suggest that denervated *Atg7* KO soleus muscles accumulate damaged mitochondria, which have reduced respiratory chain activities and produce abundant ROS.

PARK2 is required for denervation atrophy of soleus muscle

The E3 ubiquitin ligase PARK2/Parkin is commonly mutated in autosomal recessive juvenile parkinsonism.[18] Upon mitochondrial damage or uncoupling, PARK2 localizes to mitochondria and mediates the ubiquitination of mitochondrial outer membrane proteins and the autophagic elimination of damaged mitochondria (mitophagy), thereby participating in mitochondrial quality control.[19,20] Denervation induced PARK2 expression in hind-limb muscles (**Fig. 3A and B**; **Fig. S1C**) and the level of PARK2 expression induced by denervation was much higher in soleus muscles than in plantaris muscles. In addition to PARK2 expression, MFN1, a PARK2 substrate, accumulated in denervated soleus muscles from *Atg7* KO mice. In contrast, another E3 ubiquitin ligase, MUL1, which is involved in mitophagy during skeletal muscle atrophy,[21] was not induced by denervation in soleus and plantaris muscles. Subcellular fractionation experiments revealed that the mitochondrial fraction of the soleus muscles of denervated *Atg7* KO mice showed an accumulation of PARK2 (**Fig. 3C**). Immunofluorescence microscopy of cryosections of soleus muscles revealed colocalization of fragmented mitochondria and PARK2 in perinuclear regions of muscle fibers in denervated *Atg7* KO mice (**Fig. 3D**). These results indicate that damaged mitochondria associated with PARK2 are not eliminated and accumulate in the soleus muscles of denervated *Atg7* KO mice because of the deficiency of autophagy, and suggest that the contribution of PARK2 to mitochondrial clearance in denervated slow-twitch soleus muscles is much larger than it is in fast-twitch muscles, probably owing to the abundance of mitochondria. To confirm whether the PARK2-mediated mitophagy is involved in the denervation atrophy in the soleus muscles, we denervated *Park2*-deficient (*Park2* KO) mice.[22] Intriguingly, as was the case with *Atg7* KO mice, the soleus muscles from *Park2* KO mice retained muscle mass 7 d after denervation (**Fig. 1**). In

©2014 Landes Bioscience. Do not distribute.

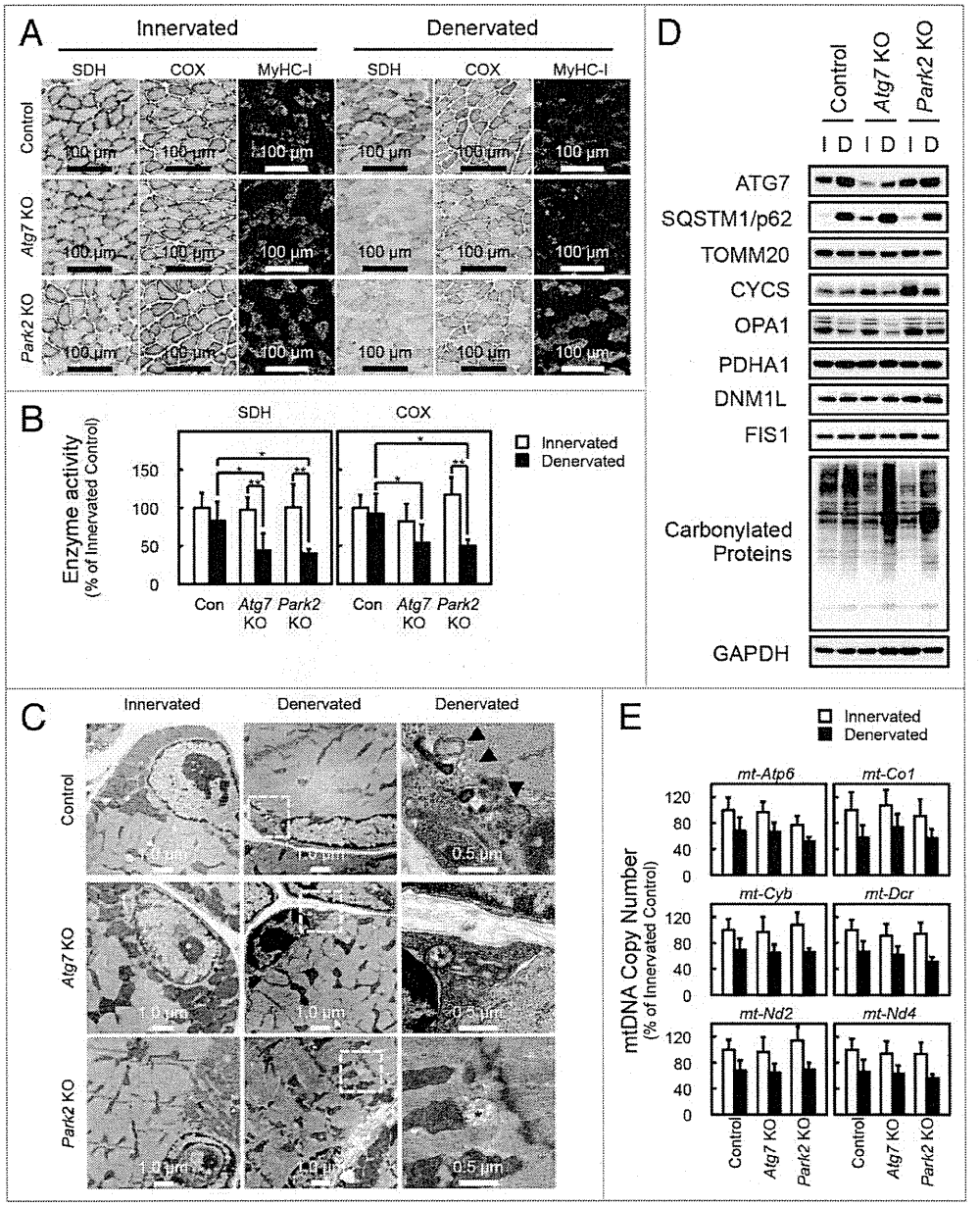

Figure 2. Denervation mediates mitochondrial damage in *Atg7* KO and *Park2* KO soleus muscles. (**A**) Histological analysis and immunofluorescence analysis of soleus muscles from control, *Atg7* KO and *Park2* KO mice 7 d after denervation. Histochemical detection of succinate dehydrogenase (SDH) and cytochrome *c* oxidase (COX) activities in cryosections of soleus muscles and immunofluorescence images of denervated soleus muscles stained with anti-myosin heavy chain I (MyHC-I, green) and anti-DMD (red) antibodies. Nuclei were visualized with Hoechst 33342 (blue). Scale bars, 100 μm. (**B**) Quantitative analysis of SDH and COX activities of soleus muscles shown in a. $^{*}P < 0.05$, $^{**}P < 0.01$. (**C**) Electron micrographs of control, *Atg7* KO and *Park2* KO soleus muscles at 7 d after denervation. Innervated limb and denervated limb are shown. The boxed regions in the middle panels are shown in the next panels on the right. Arrowhead, autophagic vacuole or phagophore membrane; asterisk, abnormal mitochondrion. (**D**) Western blot analysis of soleus muscles from mice at 7 d after denervation. Whole tissue lysates of the denervated (D) and the contralateral innervated (I) soleus muscles were immunoblotted with antibodies against the indicated proteins. The data shown are representative of at least 3 separate experiments. (**E**) Changes in mitochondrial DNA (mtDNA) copy numbers caused by denervation of soleus muscles. mtDNA copy numbers were quantified by real-time PCR to detect mtDNA-coded genes. Data are shown as the percentage of the values (mean ± s.d.) obtained from innervated soleus muscles from control mice.

©2014 Landes Bioscience. Do not distribute.

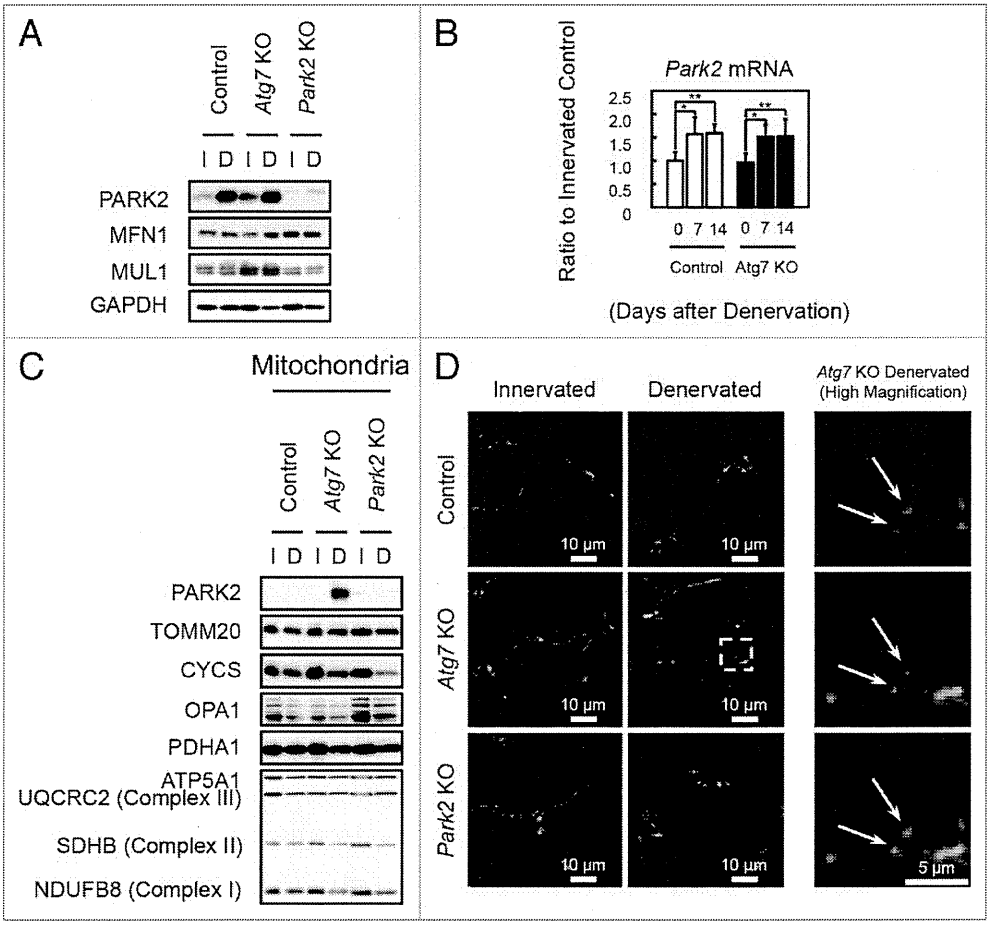

Figure 3. PARK2 accumulates in damaged mitochondria in denervated soleus muscles from *Atg7* KO mice. (**A**) Western blot analysis of soleus muscles from mice at 7 d after denervation with antibodies against the indicated proteins. (**B**) Quantification of *Park2* mRNA levels by real-time PCR in soleus muscles. Values are shown as ratios to the mRNA levels in innervated soleus muscles from control mice. The data are means ± s.d. vs. innervated (day 0) muscle from each genotype, $^{**}P < 0.01$. (**C**) Western blot analysis of mitochondrial fractions from soleus muscles. Mitochondrial fractions prepared from denervated (D) and innervated (I) soleus muscles of the indicated genotypes at 7 d after denervation and immunoblotted with anti-PARK2 antibody and antibodies against mitochondrial markers. (**D**) Immunofluorescent micrographs of denervated (7 d) or innervated soleus muscles of the indicated genotypes stained with anti-PARK2 (red) or anti-TOMM20 (mitochondrial marker, green) antibodies and Hoechst 33342 (nucleus, blue). Colocalization of fragmented mitochondria with PARK2 was observed in denervated *Atg7* KO soleus muscles. Boxed areas in denervated soleus muscles are shown in the next panels on the right.

addition, a reduction in their mitochondrial respiratory chain complex activities and accumulation of ROS were observed 7 d after denervation (**Fig. 2A–C**; **Fig. S3**). Together, these results indicate that the PARK2-mediated mitochondrial quality control pathway is required for the early stage of denervation atrophy of soleus muscles. A *Drosophila parkin*-null mutant shows obvious phenotypes including locomotive defects, muscle degeneration, and mitochondrial swelling in the flight muscles.[23-25] Indirect flight muscles, a group of specialized muscles with high mitochondria content, require a high oxygen supply to sustain their respiratory activity for a constant vibration. In mammals, slow-twitch muscles also contain more mitochondria than fast-twitch muscles. Thus, it is possible that mitochondria-rich muscles are more susceptible to the lack of PARK2-mediated mitophagy than other tissues.

PARK2-mediated mitophagy is required for proteasomal activation in denervated soleus muscle

To evaluate the mechanism underlying the delay of soleus muscle atrophy in denervated *Atg7* KO and *Park2* KO mice, we initially assumed the participation of the GDF8/myostatin signaling pathway and anti-apoptotic BCL2 family members in those phenotypes. However, denervation of wild-type, *Atg7* KO, and *Park2* KO mice resulted in very similar expression patterns for myostatin, myostatin receptor, and BCL2 family members in soleus muscles, indicating that none of these was related to the mechanism of atrophy (**Fig. S2B and S2D**). Finally, we noticed the accumulation of polyubiquitinated proteins in the soleus muscles of denervated *Atg7* KO and denervated *Park2* KO mice (**Fig. 4A**). In addition, the soleus muscles of denervated *Atg7* KO and *Park2* KO mice accumulated more polyubiquitinated proteins than did

©2014 Landes Bioscience. Do not distribute.

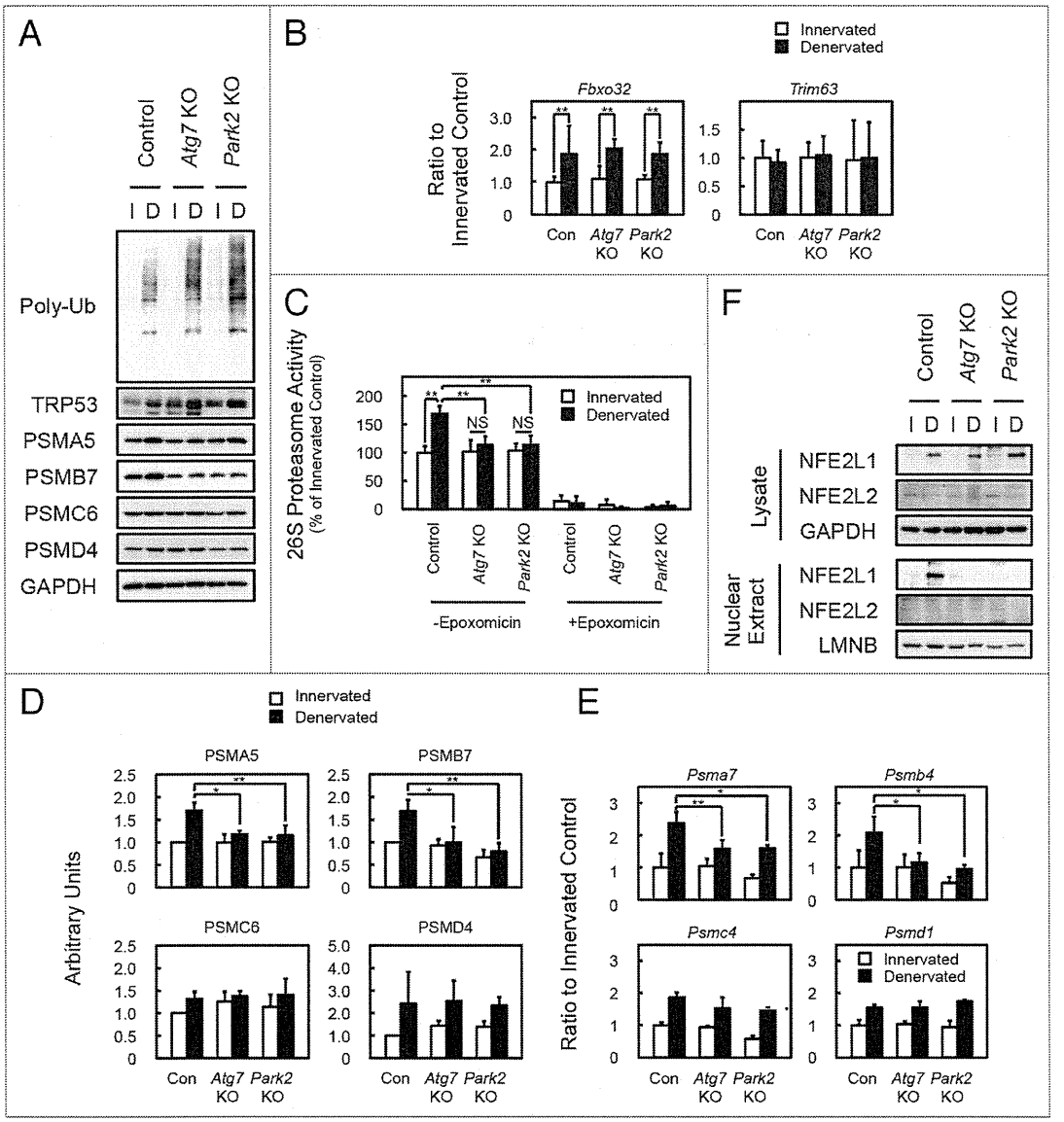

Figure 4. PARK2-mediated mitophagy is required for the activation of 26S proteasomes in denervated soleus muscle. (**A**) Western blot analysis of soleus muscles. Whole-tissue lysates of soleus muscles were immunoblotted with antibodies against the indicated proteins. The data shown are representative of at least 3 separate experiments. (**B**) Quantification of the mRNA levels for atrophy-related E3 ubiquitin ligases (*Fbxo32* and *Trim63*) in soleus muscles by real-time PCR. Data are shown as the ratios (mean ± s.d.) to the mRNA levels obtained from innervated soleus muscles from control mice. $^{**}P < 0.01$. (**C**) Peptide hydrolysis activity of 26S proteasomes. Soleus muscle homogenates from *Atg7* KO, *Park2* KO, and control mice were used to assay the chymotryptic activity of proteasomes using Suc-LLVY-AMC as a substrate in the absence or presence of 20 μM epoxomicin. Data are shown as the percentage of the activity (mean ± s.d.) obtained from innervated soleus muscles from control mice. $^{**}P < 0.01$, NS; not significant. (**D**) Quantitative densitometry of immunoblotting data for the proteasome subunits shown in a. $^{*}P < 0.05$, $^{**}P < 0.01$. (**E**) Quantification of the mRNA levels of proteasome subunits in soleus muscles by real-time PCR. Data are shown as the ratios (mean ± s.d.) to the mRNA levels obtained from innervated soleus muscles from control mice. $^{*}P < 0.05$, $^{**}P < 0.01$ vs denervated muscle from control mice. (**F**) Nuclear levels of NFE2L1 in soleus muscles. Nuclear extracts prepared from denervated and innervated soleus muscles and total tissue lysates were immunoblotted with anti-NFE2L1, anti- NFE2L2, anti-LMNB (as a loading control for nuclear extracts), and GAPDH (as a loading control for tissue lysates) antibodies. The data shown are representative of at least 3 separate experiments.

the plantaris muscles of those animals (**Fig. S4A**). It has been reported that the accumulation of polyubiquitinated proteins is a hallmark of autophagy-deficient tissues,[13-16] whereas a similar accumulation has not been reported in *Park2*-deficient animals. It is also known that the accumulation of unfolded proteins or protein aggregates interferes with proteasome-mediated protein degradation.[26,27] Therefore, we suspected that the deficiency of PARK2-mediated mitophagy attenuates the activity of the UPS pathway and results in the delay of soleus muscle atrophy in both *Atg7* KO and *Park2* KO mice. Because muscle-specific E3

©2014 Landes Bioscience. Do not distribute.

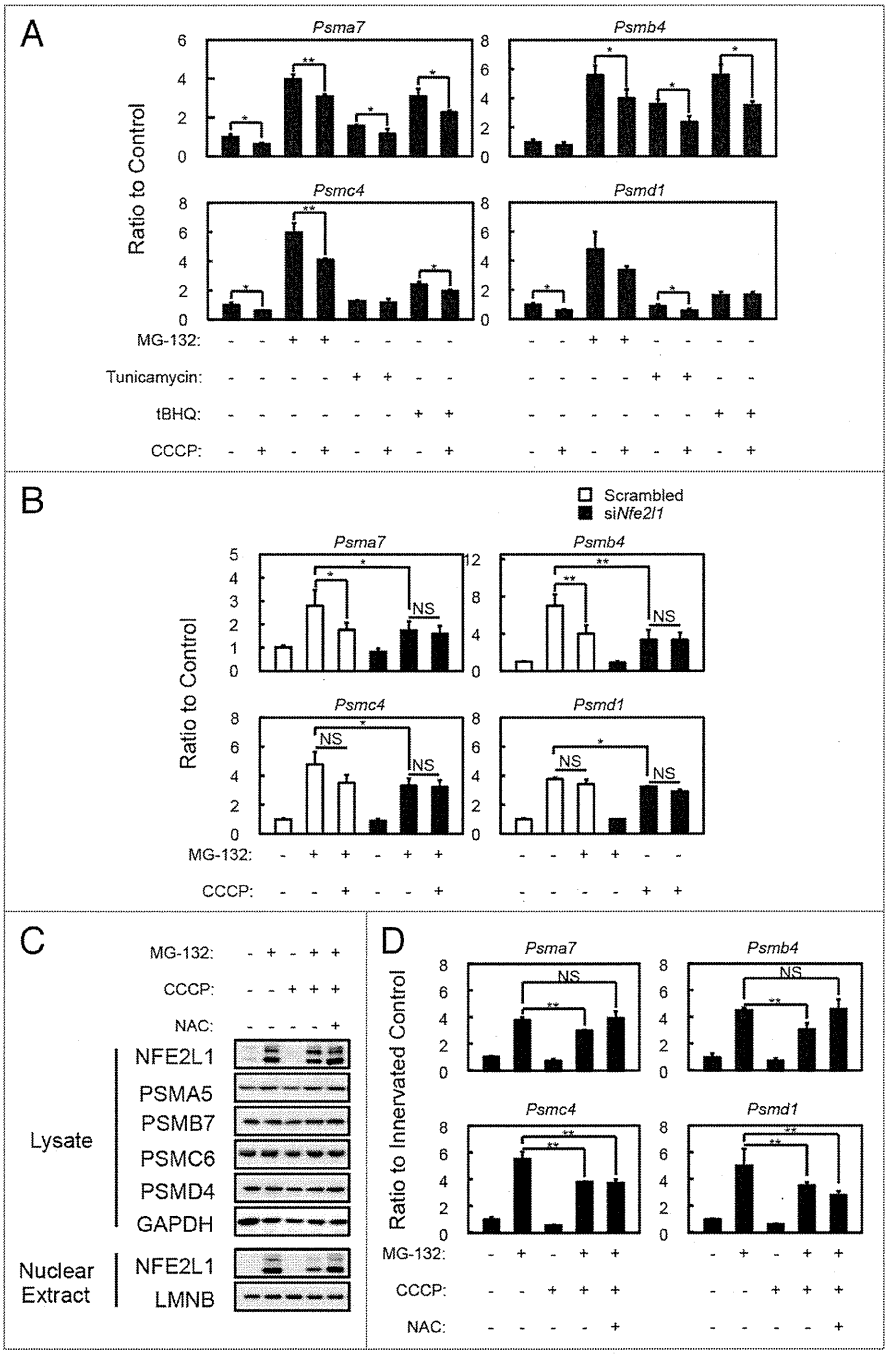

Figure 5. Effects of mitochondrial depolarization on proteasome subunit expression and NFE2L1 nuclear translocation in C2C12 cells. (**A**) Quantification of the mRNA levels of proteasome subunits in C2C12 cells incubated with 10 μM MG-132, 1 μg/ml tunicamycin and 50 μM tBHQ in the presence and absence of 10 μM CCCP for 24 h by real-time PCR. Data are shown as the ratios (mean ± s.d.) to the mRNA levels in the vehicle-treated control cells. $^{*}P < 0.05$, $^{**}P < 0.01$ (Student *t* test). (**B**) Quantification of the mRNA levels of proteasome subunits in si*Nfe2l1* treated C2C12 cells by real-time PCR. C2C12 cells were transfected with si*Nfe2l1* or scrambled siRNA, then incubated with 10 μM MG-132 in the presence and absence of 10 μM CCCP for 24 h. $^{*}P < 0.05$, $^{**}P < 0.01$, NS; not significant. (**C**) Western blot analysis of the cell lysates and nuclear extracts of C2C12 cells. Cell lysates and nuclear extracts of C2C12 cells incubated with 10 μM CCCP and/or 10 μM MG-132 in the presence or absence of 10 mM NAC for 24 h were assayed by western blotting using antibodies against the indicated proteins. The data shown are representative of at least 3 separate experiments. (**D**) Quantitative densitometry of immunoblotting data for the proteasome subunits shown in b. $^{**}P < 0.01$, NS; not significant.

ubiquitin ligases are known to promote protein degradation during skeletal muscle atrophy,[28,29] we examined the expression levels of *Fbxo32/Mafbx/atrogin-1* and *Trim63/Murf1* using real-time quantitative PCR (**Fig. 4B**). However, the expression levels of *Fbxo32* and *Trim63* in denervated soleus muscles were comparable in all of the genotypes examined. Next, we measured 26S proteasomal activities in tissue extracts from denervated and innervated soleus muscles. In control mice, denervation induced 26S proteasome activities in extracts from soleus muscles. In contrast, denervation did not induce proteasomal activation in extracts from the soleus muscles of *Atg7* KO and *Park2* KO mice (**Fig. 4C**). In addition to proteasomal activities in vitro, we found that denervation increased the levels of the endogenous proteasome substrate TRP53/p53 in the soleus muscles of *Atg7* KO and *Park2* KO mice compared with those in controls (**Fig. 4A**). In the plantaris muscles of all genotypes examined, denervation did not induce the accumulation of TRP53 as in the soleus muscles of *Atg7* KO and *Park2* KO mice (**Fig. S4A**). These results suggest that, owing to a lack of proteasome activation after denervation in the soleus muscles of *Atg7* KO and *Park2* KO mice, more TRP53 accumulated, whereas proteasome activation in the soleus muscles of denervated control mice can result in lower levels of TRP53. To ascertain whether the difference in the amount of proteasome activation caused by denervation in control and KO soleus muscles is due to an increase in the number of proteasomes, we examined protein and mRNA levels for proteasome subunits. Western blot analysis revealed that expression of the subunits of 20S proteasomes (components of the

©2014 Landes Bioscience. Do not distribute.

α and β rings) was more strongly induced by denervation in the soleus muscles of control mice than it was by denervation in the soleus muscles of *Atg7* KO and *Park2* KO mice (**Fig. 4A and D**). The mRNA levels for 20S proteasome subunits in the denervated soleus muscles from control mice were significantly higher than those in the denervated soleus muscles from *Atg7* KO and *Park2* KO mice (**Fig. 4E**). These results indicate that the deficiency of PARK2-mediated mitophagy suppresses denervation-induced transcription of 20S proteasome subunit mRNA as well as the de novo synthesis of proteasomes in soleus muscles. Interestingly, denervation induced the expression of proteasome subunits in the plantaris muscle of all genotypes examined (**Fig. S4A**). Therefore, denervated plantaris muscles of *Atg7* KO mice atrophied to almost the same extent seen in denervated plantaris muscles of control mice (**Fig. S1A**).

Accumulation of damaged mitochondria suppresses NFE2L1 transcriptional activity

Nuclear factor erythroid-derived 2-related factors (Nrfs; NFE2L1/Nrf1/TCF11/LCRF1 and NFE2L2/Nrf2), cap'n'collar-type basic leucine zipper (CNC-bZip) protein family members, have been reported to regulate the transcription of proteasome subunits.[30-33] Nrfs bind to the antioxidant response element (ARE) in the promoters of its target genes.[34] The promoters of all mammalian proteasome subunits contain ARE or ARE-like sequences.[32] To ascertain whether there were any differences in the Nrfs levels of the soleus muscles of control and *Atg7* or *Park2* KO mice, we examined Nrfs levels in tissue lysates and the nuclear extracts of soleus muscles by western blotting analysis (**Fig. 4F**). Denervation elevated total NFE2L1 levels in the soleus muscles of all genotypes examined, whereas, the NFE2L1 level was high in the nuclear extracts of soleus muscles of denervated control mice, but very low in those of the innervated control and denervated *Atg7* or *Park2* KO mice. In contrast, little NFE2L2 was detected in total lysate and nuclear extracts from soleus muscles. However, denervation did not influence the NFE2L1 levels in tissue lysates, and decreased nuclear NFE2L1 levels in the plantaris muscles of all genotypes examined (**Fig. S4C**). Although total NFE2L2 levels in plantaris muscles were comparable to those in soleus muscles, denervation elevated the NFE2L2 level in nuclear extracts of the plantaris muscles of all genotypes examined. These results indicate that 2 different Nrfs, NFE2L1 and NFE2L2, are involved in the denervation-induced expression of proteasome subunits in slow-twitch soleus muscle and fast-twitch plantaris muscle, respectively.

To confirm that the accumulation of damaged (or uncoupled) mitochondria in the soleus muscles of denervated *Atg7* KO or *Park2* KO mice affects NFE2L1 nuclear translocation, we treated C2C12 cells, a murine myoblast cell line, with the mitochondrial uncoupler carbonyl cyanide m-chlorophenylhydrazone (CCCP) to induce a mimetic condition of damaged mitochondria accumulation, and examined its effect on NFE2L1 transcriptional activity. As previously reported, incubation with several drugs, including proteasome inhibitors (MG-132), tunicamycin and tert-butyl hydroquinone (tBHQ), promotes mRNA expression of proteasome subunits (especially 20S proteasome components)[32,33,35,36] (**Fig. 5A**), and the expression of the 20S proteasome subunits induced by those drugs was suppressed by the addition of CCCP. In addition, siRNA knockdown of *Nfe2l1* significantly suppressed MG-132-induced proteasome subunit expression (**Fig. 5B**) Moreover, MG-132-induced NFE2L1 nuclear translocation was also suppressed by the addition of CCCP in C2C12 and HeLa cells (**Fig. 5C and D**; **Fig. S5C**). In addition, the effects of CCCP on MG-132-induced NFE2L1 nuclear translocation and NFE2L1 target-gene expression were blocked by the addition of N-acetyl-cysteine (NAC), an antioxidant. These results indicate that 24 h CCCP treatment induces ROS production from mitochondria in addition to the mitochondrial depolarization. To confirm the effect of ROS on NFE2L1 nuclear translocation, we tested the effects of rotenone, a complex I inhibitor, antimycin, a complex III inhibitor, and H_2O_2 on nuclear levels of NFE2L1 (**Fig. S5A and S5B**). As expected, the addition of rotenone, antimycin or H_2O_2 suppressed the MG-132-induced NFE2L1 nuclear translocation, and the effects of those drugs were invalidated by the addition of NAC. Together, these results indicate that the accumulation of damaged mitochondria producing ROS negatively affects NFE2L1 translocation and the transcription of NFE2L1 target genes.

Discussion

Mitochondria have been postulated to play an important role in triggering signals that contribute to muscle atrophy.[37] In this study, we noticed that a similar pattern of mitochondrial dysfunction and soleus muscle atrophy in denervated autophagy-deficient and *Park2*-deficient mice, and showed the evidence for PARK2-mediated mitophagy playing the important roles in slow-twitch muscle atrophy, which is the first report showing the physiological role of the PARK2-mediated mitophagy in mammalian in vivo model. The accumulation of damaged mitochondria in the PARK2-mediated mitophagy deficient soleus muscle, interferes the expression of proteasome subunits (**Fig. S6**). The elevation of proteasome expression is the key event in the early stage of slow-twitch muscle atrophy, and that it is regulated by a transcription factor NFE2L1. Under nonstress conditions, NFE2L1 is targeted by its N-terminal putative transmembrane domain to the endoplasmic reticulum (ER) membrane, where it is quickly degraded via ER-associated degradation (ERAD).[33,35,38] In response to proteasome inhibition, NFE2L1 translocates from the ER to the nucleus, where it transactivates the transcription of target genes including proteasome subunits. Conversely, NFE2L2, another Nrfs, is constitutively degraded by proteasome because its binding partner KEAP1 (kelch-like ECH-associated protein 1) is a component of the ubiquitin ligase complex in standard conditions.[39-42] The oxidative and electrophilic stresses inactivate KEAP1 by the modification of its cysteine residues, and stabilize NFE2L2 to induce the transcription of numerous cytoprotective genes.[43-45] In this study, we showed that NFE2L1 nuclear translocation is interfered by oxidative stress, which activates NFE2L2 activity. Therefore, the PARK2-mediated mitochondrial quality control system plays an important role

©2014 Landes Bioscience. Do not distribute.